14 In Vivo Intrinsic Optical Signal Imaging of Neocortical Epilepsy

SONYA BAHAR, PhD, MINAH SUH, PhD, ASHESH MEHTA, MD, PhD, AND THEODORE H. SCHWARTZ, MD

SUMMARY

Intrinsic optical signal (IOS) imaging is a technique for measuring changes in blood flow, metabolism, and cellular swelling associated with neuronal activity. The combined spatial and temporal resolution, in addition to the ability to sample large areas of cortex simultaneously, make it a powerful technique for brain mapping. IOS has only recently been applied systematically to the study of epilepsy. This chapter will explore the utility and feasibility of mapping interictal spikes, ictal onsets, offsets, and horizontal propagation using IOS imaging in acute and chronic animal models of epilepsy. The implementation of IOS imaging in the operating room during neurosurgical procedures will be discussed as well as technical challenges that currently restrict this translational work to a very few centers.

Key Words: Epilepsy; optical imaging; intrinsic signal; rat; ferret; seizure; ictal; interictal; iron; tetanus toxin; human; surgery.

1. BACKGROUND

1.1. HISTORICAL BACKGROUND AND PHYSIOLOGICAL ORIGIN OF THE INTRINSIC OPTICAL SIGNAL

Intrinsic optical changes in neural tissue were first observed by Hill and Keynes (*1*; *see* also refs. *2* and *3*) in response to an applied train of stimuli and later in response to single electrical stimuli (*4*; *see* ref. *5* for review). Only recently, however, has the intrinsic optical signal (IOS) been systematically applied to the study of the nervous system. A decrease in light reflectance has been shown to correlate spatially with increased electrophysiological activity *(6–8)*.

The IOS has several distinct advantages: first, it offers high spatial resolution, to a level of approx 50 μm *(7, 9)*. In contrast, the spatial resolution of functional magnetic resonance imaging (fMRI) is 1 mm *(10)*. Second, because it does not involve the application of potentially phototoxic dyes, it is a minimally invasive technique and thus well suited to applications involving the intraoperative imaging of human patients or long-term in vivo animal studies. In contrast to voltage-sensitive dyes and calcium-sensitive dyes, however, the time-course of the change in light reflectance is considerably slower than the time-course of single action potentials or field potentials *(11,12)*. This suggests that the intrinsic signal demonstrates physiological changes caused by the underlying electrophysiology rather than reflecting the electrophysiology itself *(11,12)*.

The IOS derives from changes in the light absorbance properties of electrophysiologically active neural tissue, caused by focal alterations in blood flow, oxygenation of hemoglobin, and scattering of light *(13,14)*. The amplitude and time-course of the IOS are dependent on the wavelength of incident light *(13,14)*. Multiwavelength imaging in striate cortex during visual activation has demonstrated that the IOS recorded at different wavelengths represents separate cortical processes, each associated indirectly with neuronal activity. Around the isosbestic wavelengths of hemoglobin, roughly 480–590 nm, the signal is most sensitive to blood volume *(13)*. At higher wavelengths, from 600–650 nm, the signal is dominated by the oxygenation state of hemoglobin. Finally, at wavelengths greater than 660 nm, the light-scattering component created by fluid shifts becomes dominant *(14)*. Although the signal is never "pure," and at each wavelength there are contributions from each component, a high spatial correlation with neuronal activity has been well demonstrated in multiple animal preparations in various regions of cortex.

The exact physiological components of the IOS recorded at each wavelength are not yet fully understood. There is general agreement that as neurons become activated, they increase their metabolic demand causing an increase in the concentration of deoxyhemoglobin *(14–16)*. This "initial dip" in local oxygenation is spatially highly colocalized with neuronal activity and begins within 100 ms of neuronal activation *(13)*. Simultaneously, the opening of sodium, potassium, and calcium channels causes a change in the volume of cells and the extracellular

From: *Bioimaging in Neurodegeneration*
Edited by P. A. Broderick, D. N. Rahni, and E. H. Kolodny

fluid as well as swelling of glia, which buffer extracellular potassium. These fluid shifts are also spatially well colocalized with neuronal activity. Approximately 300–500 ms later, the arterial microvasculature begins to dilate and cause an increase in blood volume, which is not as well localized with neuronal activity *(14)*. Finally, between 0.5 and 1.5 s later, there is an activity-dependent increase in blood flow that delivers oxygenated blood to the area. This increase in blood flow causes an increase in oxygenation because the incoming oxygenated hemoglobin overwhelms the metabolic needs of the neurons *(17)*. This later component causes an inverted optical signal in the larger blood vessels and is the basis of the blood oxygen level-dependent (BOLD) signal imaged with low-tesla fMRI (i.e., 1.5 T; refs. *15*,*16*,*18*). Colocalization of this process with neuronal activity is less precise and often seen in the draining veins *(16)*.

1.2. USE OF THE IOS IN IMAGING FUNCTIONAL ARCHITECTURE

Because of its high spatial resolution and slow time course, the IOS was initially applied to the mapping of functional architecture in the cortex. In this arena, the IOS proved spectacularly successful. In fact, it was using this technique that it was first demonstrated that iso-orientation domains in the cat visual cortex are arranged in a pinwheel-like structure *(7)*. Numerous other studies have since been conducted in the visual cortex using the IOS in the mouse *(19)*, cat *(6,20–23)*, ferret *(24–27)*, tree shrew *(28,29)* and nonhuman primate *(30,31)*. Because the signal is extremely small (~0.1%), these studies rely on signal averaging and trial repetition to improve the signal-to-noise ratio. In general, trials in which the cortex is activated by a known stimulus are divided by, or subtracted from, trials without activation *(32)*. Novel techniques for image processing such as Fourier transform (FT) and principal component analysis (PCA)-based methods are also being investigated to eliminate the need for image division *(33,34)*.

Figure 1 shows the orientation columns and ocular dominance columns imaged from a ferret. In such a typical functional architecture study, images are taken from the exposed cortex of the ferret while it is viewing moving gratings at different angles on a video screen through each eye while the other eye is covered. To map the areas that respond to a given orientation, the IOS obtained during stimulus with a given condition (grating at a certain angle) is divided by a signal averaged from the responses of the animal to a variety of stimuli (gratings at all different angles, the so-called "cocktail blank"). Ocular dominance columns are obtained by dividing all images acquired when one eye is open by those acquired when the other is open.

Other regions of functional cortex, ranging from the rodent barrel cortex *(13,35–37)* to somatosensory cortex in the nonhuman primate *(38–40)* have been mapped as well. Technical advances in the development of an "artificial dura" have made chronic imaging of awake, behaving animals a reality *(41)*.

1.3. USE OF IOS FOR IMAGING DYNAMIC EVENTS: FROM SPREADING DEPRESSION TO EPILEPSY

In addition to its use in mapping static functional architecture, however, the IOS also can be used for the study of dynamic events. The critical difference between imaging static architecture and dynamic processes is that multiple trials cannot be averaged together. Events such as spreading depression and seizures are not only dynamic, in that they move across the cortex over time, but sequential events are not necessarily stereotypical and can spread along different pathways and at different rates. Because events cannot be averaged, the signal would be very difficult to see using image division techniques if it were the same size as physiologic sensory activation. Luckily, the IOS associated with spreading depression, interictal spikes, and ictal events is anywhere from 5 to 500 times as large as found with physiologic sensory activation. Even so, averaging is occasionally possible, even with dynamic events, as in the case of certain models of interictal spiking, as will be discussed below.

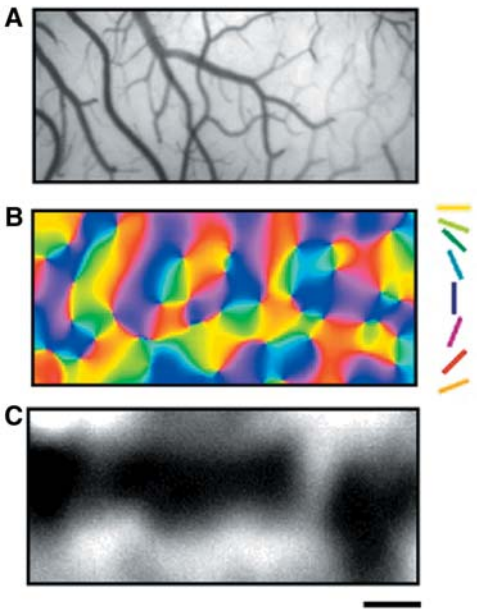

Fig. 1. Optical imaging of intrinsic signals reveals the functional architecture in ferret visual cortex. **(A)** Blood vessel pattern of the surface of the visual cortex imaged at 546 nm. **(B)** The angle map is generated by color-coded vectorial summation of each single condition (0, 45, 90, 135, 180, 225, 270, 315, and 360°) map on a pixel-by-pixel basis. **(C)** Ocular dominance columns are obtained by dividing images acquired with one eye covered by those acquired with the other eye covered. Imaging performed at 707 nm. Scale bar, 1 mm.

1.3.1. Spreading Depression

Cortical spreading depression (CSD), first studied by Leão *(42,43)*, consists of a sharp drop in the DC potential ("DC shift", typically 10-20 mV) that spreads across the cortex at a rate of up to 10 mm/min *(44)* and also can be accompanied by a depression of the EEG and suppression of evoked potentials *(42,43)*. CSD can occur in response to noxious stimuli such as direct mechani-

cal injury *(42,43,45,46)*, application of glutamate *(47)*, elevated potassium *(48)*, electrical stimulation *(43)*, or hypoxia *(49)*.

CSD has been studied with IOS imaging in the visual system *(50)*, rat hippocampal slices *(51,52)*, and the rat neocortex in vivo *(46,53)*. The initial CSD-related IOS response consists of a decrease in light reflectance in vivo (often observed as an increase in light transmittance in slice experiments). This is followed by a sharp rise in reflectance (decrease in transmittance) that propagates in a wave-like fashion through the tissue; the leading edge of this "wave" coincides spatially with the DC shift *(49,51)*.

1.3.2. Epilepsy

Epilepsy is a chronic neurological disease that affects as much as 2% of the population with recurrent seizures *(54)*. Seizures, or "ictal events," consist of the paroxysmal, synchronous, rhythmic firing of a population of pathologically interconnected neurons capable of demonstrating high-frequency oscillatory activity called "fast ripples" (250–500 Hz; refs. *55–57*), synchronized by axo-axonal gap junctions, field effects or interneurons *(58–60)*. These events are caused by an imbalance in excitatory and inhibitory mechanisms leading to both hypersynchrony and hyperexcitability *(61)*. The role of inhibition in the etiology of epileptiform events, however, is controversial and quite relevant to optical imaging studies. Because epileptiform activity is characterized by a hyperexcitable, hypersynchronous state, classic hypotheses often supposed a decrease in inhibitory tone in the region of the epileptic focus. In agreement with this theory, administration of GABA-A antagonists such as penicillin or bicuculline induces acute epileptiform events in vitro and in vivo *(62–70)*. Likewise, losses of several subtypes of interneurons are reported in both experimental and human temporal lobe epilepsy *(71)*. However, there is a great deal of evidence that inhibitory mechanisms are functionally unaltered or even increased in several non-lesional chronic in vivo and in vitro models *(72–76)*, as well as human epileptic tissue, studied both in vivo and in vitro *(73,77,78)*.

The role of inhibitory processes in the prevention of epileptic events also is unclear. In certain models of acute epilepsy, electrophysiologic recordings from brain surrounding the epileptic focus demonstrate upregulated inhibition, the so-called "inhibitory surround." First described by Prince in the acute disinhibition model , the inhibitory surround develops several minutes after the initiation of bursting in the focus and was thought to be generated by long-range horizontal inhibitory connections, presumably mediated by basket cells, which are recruited by bursting cells in the focus *(79–83)*. Alternatively, long-range horizontal excitatory connections recently have been shown to powerfully recruit local inhibitory circuitry in response to focal repetitive stimulation in tangential slices *(84,85)*. Surround inhibition has been hypothesized to play a role in preventing interictal to ictal transition, secondary generalization of focal ictal events, and may explain the profound interictal focal hypometabolism/hypoperfusion found in most functional imaging studies performed in chronic human epilepsy *(72,82,86)*. Although not well-described in human epilepsy or experimental chronic models of epileptogenesis, more recent experimental evidence demonstrates an inhibitory surround restricting the size of cortex capable of generating fast ripples in the hippocampus of kainate treated rats *(56)*.

When seizures are not occurring, surface recordings from patients with chronic epilepsy, or intracortical field potential (f.p.) recordings adjacent to experimentally induced epilepsy in laboratory animals, show abnormal paroxysmal events in a large population of neurons called interictal spikes (IIS). The IIS generally consists of a high amplitude surface negativity (1–5 mV) lasting 50–200 ms followed by a slow wave with no behavioral correlate *(87)*. The intracellular event underlying the IIS, explored in a variety of animal models, consists of a large paroxysmal depolarizing shift (PDS) with a superimposed burst of action potentials that occurs in a variable percentage of the adjacent neurons depending on the etiology of the epilepsy, followed by an afterhyperpolarization *(62,88–92)*. The transition to an ictal event, or seizure, occurs when the afterhyperpolarization gradually disappears and is replaced by further depolarization *(88,89)*.

1.3.3. IOS Imaging of Neocortical Epilepsy

Because epileptiform events involve synchronous activity in a large population of neurons with associated changes in blood flow, metabolism, and shifts in extracellular ions and fluids, the associated IOS should be enormous. In fact, Wilder Penfield, a pioneer epilepsy neurosurgeon, commented in the 1930s that he could grossly perceive focal dilation in local vasculature associated with neocortical seizures in the operating room with the naked eye *(93)*. IOS imaging has been applied to the study of epileptogenesis in the slice preparation *(94–97)*, isolated guinea pig whole brain *(98)*, in vivo rat *(99)*, ferret *(100)*, nonhuman primate *(101)*, and human *(102)*. The first report of using IOS imaging to map epilepsy in vivo was performed in humans by Haglund et al. in 1992 *(102)*. They triggered afterdischarges with a bipolar stimulating electrode and optically recorded the IOS at 610 nm. In addition to noting the large amplitude of the signal, they described an "inverted" optical signal recorded from the adjacent brain, which was hypothesized to represent either surround inhibition or shunting of blood flow from adjacent cortex. The first report of in vivo imaging of pharmacologically induced spontaneous (not electrically triggered) epileptiform events with simultaneous electrophysiological monitoring was by Schwartz and Bonhoeffer *(100)*. In their study in ferret visual cortex at 707 nm, both interictal and ictal events were induced pharmacologically. With simultaneous field potential recordings, the precise time and morphology of the epileptiform event was correlated with the optical signal. They also confirmed the inverted optical signal from surrounding cortex and demonstrated a decrease in neuronal activity with single-unit recordings. In this work, they also described the first imaging of a mirror focus in contralateral homotopic cortex. Chen et al. *(99)* reported IOS imaging of penicillin-induced seizures in the rat and raised the possibility that the IOS may be able to predict seizure onset as early as 1 min before an electrographic event, which has not been confirmed by other groups. Finally, Schwartz *(27)* reported simultaneous optical imaging of epileptiform events and functional architecture in ferret visual cortex.

1.4. THEORETICAL BASIS FOR CLINICAL UTILITY OF IOS IMAGING IN THE TREATMENT OF EPILEPSY

The epilepsies are categorized based on the location of the region of brain involved at the onset of the seizure. Focal or

"partial" seizures begin in localized, abnormal areas of the brain. These epileptic events can secondarily generalize by propagating through more normal areas and sequentially recruiting additional neuronal populations. Currently, the only known cure for epilepsy is surgical removal of the epileptic focus. It is estimated that there are more than 100,000 currently untreated surgical candidates with partial epilepsy with 5000 new candidates each year *(103)*. Partial epilepsies can start in either the medial temporal lobe structure or the neocortex. Surgery is only curative in partial epilepsy, and the key to successful outcome is the ability to localize the epileptic focus. IOS imaging is most useful in imaging the neocortex since it is easily exposed and hence only neocortical epilepsy will be discussed in this chapter.

The current gold standard in mapping epilepsy uses electrophysiologic recordings from the surface of the brain. Surface electrographic techniques such as electroencephalography (EEG) and electrocorticography (ECoG) record field waves generated by membrane currents of coactive neurons passing though the extracellular space. These field potentials reflect the linear sum of fields generated by current sources (current from the intracellular space to the extracellular space) and sinks (current from the extracellular space to the intracellular space; ref. *104*). The predominant sources of these fields are slow synaptic and nonsynaptic events. Because the principles of field recording are based on volume conduction, and the cortex can be modeled as a convoluted dipole layer *(105)*, the relationship between the size of the potential at a given point and the distance of the point from the generator is not straightforward. This severely undermines the localizing value of field recordings *(105)*. In addition, differentiating volume conduction from neurophysiological propagation with surface recordings is quite difficult *(106)*. Action potentials contribute little to field recordings unless the electrode is in very close proximity to a large population of synchronously bursting neurons. However, simultaneous extracellular and surface recordings from models of chronic epileptogenesis have shown that surface recording techniques do not localize the activity of bursting "epileptic" neurons. Hence, surface spikes may be a propagated phenomenon only loosely co-localized with the epileptogenic region *(90)*.

This raises the intriguing possibility that IOS imaging may actually be a better, or at least complementary, technique for localizing the epileptic focus and thus may potentially help guide surgical resections. Preliminary evidence for this conclusion was reported by Schwartz and Bonhoeffer *(100)*, who found that the surface ECoG was insensitive to interictal spikes that could be recorded with both a local field potential and IOS imaging. Likewise, the report by Chen et al. *(99)* that IOS may be a useful predictor of epileptiform events increases the potential clinical utility of the technique. Optically recorded changes in cytosolic free calcium in vivo were also noted approx 20 s before electrophysiological events, further supporting the notion that optical imaging techniques may be more sensitive to pre-epileptiform events and useful in predicting seizure onset *(107)*.

In the remainder of this chapter, we will present recent advances in the imaging of interictal and ictal events in vivo in the ferret and rat (Subheading 2) and discuss the current state of the use of IOS imaging for intraoperative human imaging (Subheading 3). Our focus will be the work done in our laboratory.

2. OPTICAL IMAGING OF ANIMAL MODELS OF EPILEPSY

2.1. BACKGROUND

Because the bulk of the experiments in this study were performed on animal models of epileptogenesis, it will be helpful to review our current understanding of the pathophysiology of those models relevant to this study. Because few animals develop spontaneous seizures, none of these models are fully trustworthy as an imitation of clinical epilepsy *(108,109)*. However, each provides a well-controlled environment for exploring different aspects of epileptogenesis. Acute models, in particular, have been extensively studied but lack several of the key components that characterize more chronic models and human epileptogenesis . We use acute models to address questions regarding the relationship between the optical signal and the underlying electrophysiology because they have been extensively studied and their pathophysiology is well understood. Chronic models are useful to investigate specific questions relevant to human epileptogenesis that cannot be studied in patients for ethical reasons.

2.1.1. Acute in Vivo Rodent Models

Acute models of neocortical interictal events in the rodent usually involve either the focal intracortical application of GABA-A antagonists, such as penicillin or bicuculline methiodide (BMI), or cryogenic injury *(109,110)*. Neocortical ictal events, however, can be precipitated either by application of 4-aminopyridine (4-AP) or direct cortical stimulation producing afterdischarges *(111–113)*.

2.1.1.1. The Disinhibition Model

Intracortical injection of GABA-A antagonists induces stereotypical IIS at a frequency of 0.2–0.7 Hz in many animals, including the nonhuman primate, cat, ferret, rabbit, rat, and mouse *(62,64,100,109,110,114–116)*. Intracellular recordings from within the focus reveal that a majority of neurons sampled exhibit a paroxysmal depolarization shift (PDS) simultaneous with the IIS recorded from the local f.p. *(62–64,83)*. Intracellular recordings from neurons at variable distances from the center of the focus reveal varying degrees of activity ranging from a sustained PDS in the center, to a truncated PDS at the margin, to subthreshold EPSPs, to brief EPSPs, followed by an IPSP and prolonged IPSPs in the surrounding cortex, representing the so-called "inhibitory surround" (*81–83,117*). Whether surround inhibition is an essential component of the epileptic focus or only found in the acute pharmacologically disinhibited focus is controversial. Although the acute disinhibited model of epileptogenesis has been historically the most widely used model, it has several disadvantages. Although there is some evidence that GABAergic circuitry and pharmacology may be reduced in human epilepsy, it is not necessary for epileptogenesis and is even upregulated in many models of chronic epileptogenesis (*see* Subheading 1.3.2.; ref. *72*). The intensity of the focus as manifested in the large percentage of neuronal participation in the IIS is not seen in neurons in human foci studied with extracellular recordings during neuro-

surgical operations *(118–120)*. Likewise, the inhibitory surround has not been described in either human or chronic models of epileptogenesis, although few studies have directly examined this question *(91,120)*.

2.1.1.2. The 4-AP Model

4-AP is a potent convulsant when applied to the neocortex *(121)*. It has many mechanisms of action, most of which act to increase synaptic transmission. At doses less than 10 μ*M*, it acts by blocking slowly inactivating potassium currents *(122)* and enhances the release of synaptic neurotransmitters *(123,124)*. At higher doses, it enhances calcium currents at synaptic terminals *(125)*. In contrast to its effect in the slice preparation, in which interictal events are produced, application to the neocortex in vivo generates tonic-clonic ictal electrographic seizures *(111,112,126)*. Events last anywhere from 60–300 s with interictal periods of 5–20 min *(111,112,126)*. Ictal events begin focally at the point of application and spread horizontally in a symmetric, reproducible fashion *(100,127,128)*. In contrast to interictal models, intracellular recordings reveal little correlation between depolarizing potentials and surface paroxysmal discharges *(126)*. These findings are reminiscent of more chronic models of epilepsy as well the human situation. The 4-AP model is the best acute model of ictal events and is particularly useful for examining the relative localization of ictal onset versus offset as well as the relationship between the optical recording and surface electrophysiological recording of horizontally propagating seizures.

2.2. IOS IMAGING OF INTERICTAL SPIKES

We have performed IOS imaging of IIS using the acute disinhibition model in both ferrets and rats. It was originally unclear if such a slow signal like the IOS had sufficient temporal resolution to map the IIS, which spreads across the cortex at a rate of approx 80 mm/s *(67,129)*. In fact, the electrophysiologic spread of the IIS is far too rapid to be resolved with the IOS. However, as will be demonstrated, if the time between each IIS is sufficient for the intrinsic signal to rise and fall back to near baseline, and the lateral spread of each IIS is smaller than the region of exposed cortex, the spatial extent of each IIS can be easily resolved with the IOS.

2.2.1. Animal Surgery

For the ferrets, anesthesia was induced with a mixture of ketamine (15–30 mg/kg i.m.) and xylazine (1.5–2.0 mg/kg i.m.) supplemented with atropine (0.15 mg/kg i.m). After tracheotomy, animals were ventilated with 60–70% N_2O, 30–40% O_2, and 1.4–1.6% halothane (halothane was reduced to 0.8–0.9% for the imaging) and placed in a stereotactic frame. End-tidal CO_2 was maintained at 3.2–3.8% and animals were hydrated with 2 mL/kg/h dextrose/Ringer's solution and paralyzed with intravenous gallamine triethiodide (30 mg/kg/h). For the rat studies, adult male Sprague–Dawley rats (250–375 g) were initially anesthetized with an intraperitoneal (i.p.) injection of a cocktail of 90 mg/kg ketamine and 4.0 mg/kg xylazine. After induction, the trachea was cannulated and anesthesia maintained with i.p. injection of 1.3 g/kg urethane. Animals were placed in a stereotactic frame and hydrated with i.p. 2 mL/kg/h dextrose/Ringer's solution. Supplementary anesthesia was administered on occasion as needed, depending on the animal's reflex response to a toe-pinch. Oxygen saturation and end-tidal CO_2 were monitored and kept constant at 100% and 3.5%, respectively. In both preparations, dexamethasone (0.1 mg/kg; Steris Laboratories, Phoenix, AZ) and atropine (0.5 g/kg; Atroject; Burns, Rockville, NY) were administered subcutaneously. ECG and rectal temperature were continually monitored and temperature was maintained at 37°C by means of a homeothermic blanket system (Harvard Apparatus, Holliston, MA). For the ferrets, a craniotomy was performed over visual cortex with a high-speed dental drill and the dura was opened. For the rats, the skull was thinned and a small hole made in the skull and dura over the hindpaw somatosensory area (Fig. 2).

2.2.2. Electrophysiology and Epileptogenesis

Epidural ECoG was performed with two electrodes on either side of the craniotomy, approx 5 mm from the epileptic focus. In both preparations, two glass micropipets were advanced into layers II-III with micromanipulators. One micropipet was filled with 1% NaCl for field potential recording. A second micropipette with a tip resistance of 4–6 MΦ, filled with a solution of bicuculline methiodide (5 m*M* in 165 m*M* NaCl, pH 3.0), was positioned less than 1 mm from the field potential electrode. ECoG and f.p. signals were amplified, bandpass filtered (1–100 Hz), and digitized at 200 Hz (ferret) or 2000 Hz (rat) and recorded onto a PC.

Interictal foci were induced by iontophoresis of BMI using a current of –15 to –20 nA for retention and +50 to +500 nA for release depending on the resistance of the micropipette tip. Positive currents were maintained until stereotypical IIS were recorded (after ~5 min).

2.2.3. IOS Imaging

2% agar and a glass coverslip were placed over the cortex for stabilization. For the ferret experiments, the brain was illuminated by a halogen lamp filtered to 707 ± 10 nm through two fiberoptic light guides. For the rat experiments, illumination was at 546 ± 10 nm, 605 ± 10 nm, 630 ± 10 nm, and 700 ± 10 nm. In the ferret, the optical reflectance signal was recorded at 2 Hz with a cooled CCD camera (ORA 2001, Optical Imaging Inc., Germantown, NY) equipped with a tandem lens *(130)*, focused approx 500 μm beneath the cortical surface. For the rat, the optical signal was recorded with a 10-bit video camera (Imager 3001, Optical Imaging Inc., Germantown, NY) at 10 Hz.

Image processing was done with custom software written in either IDL (Research Systems, Inc) or MATLAB (The MathWorks, Inc.) was used to generate the epilepsy maps. Blank-divided (BD) maps were produced by dividing each frame acquired during epileptic conditions from control images obtained with a negative holding current. Spike-triggered (ST) epilepsy maps were obtained by dividing single frames following the epileptic event by the single frame preceding the event. These maps could be averaged over multiple events since the IIS is so stereotypical. To determine the spatial extent of each epileptiform event, we used the method of normalized threshold analysis developed by Chen-Bee et al. *(131)* and others *(35,132)*. For a given set of images, the dynamic range of pixel intensities (minimum to maximum) was determined. Each pixel was then evaluated to determine whether it was a given percentile of the dynamic range below the median pixel intensity. The median was used instead of the mean because it is less

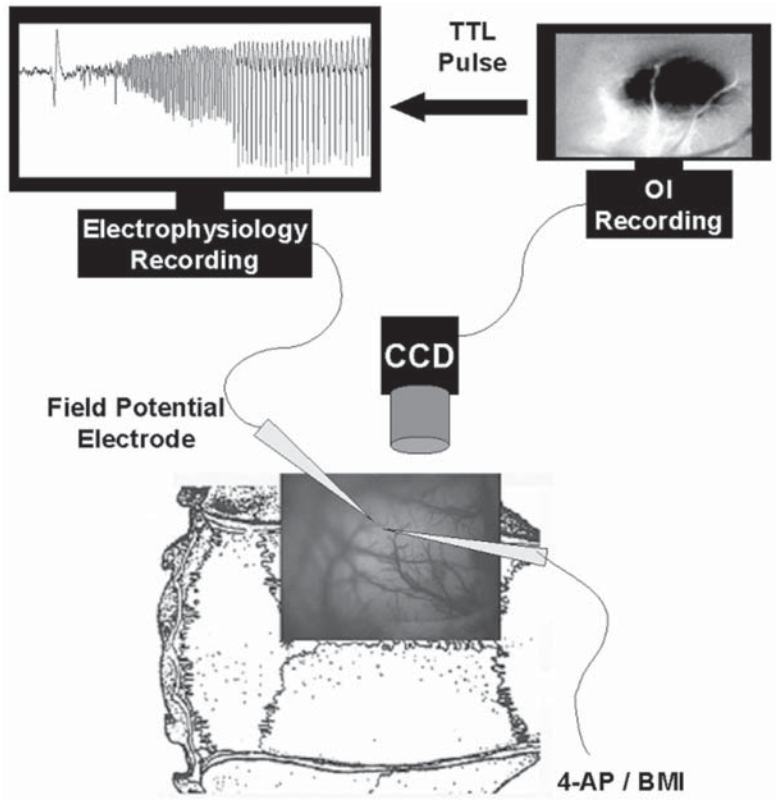

Fig. 2. Schematic diagram of the experimental setup for in vivo optical imaging in the rat neocortex. At bottom, the rat brain is exposed and one side of the skull over the neocortex is thinned. A small hole is made in the thinned skull and the dura below, and a field potential electrode is inserted, along with a second electrode, through which a pharmacological agent may be injected to cause ictal or interictal events. The field potential signal is continuously recorded. Images are collected by the CCD camera placed and digitized onto a PC. A TTL pulse from the imaging computer is fed into the computer that records the electrophysiology mark each frame acquisition, so that the imaging and the interictal or ictal events can be temporally correlated during off-line analysis.

sensitive to outliers. Note that this procedure also can be used to determine the size of the region of increased light reflectance (i.e., inverted optical signal in the putative inhibitory surround), by evaluating which pixels are at a given percentile of the dynamic range *above* the median. The determination of spatial extent as just defined can be performed using any given percentile of the dynamic range ("threshold"). With higher thresholds, the criterion for determining whether a given pixel is part of the seizure is more stringent, and thus as the threshold is increased, the seizure will appear "smaller." Hence, the calculated area is somewhat arbitrary.

2.2.4. Single Wavelength Imaging in the Ferret

In the first report of simultaneous electrophysiology and IOS imaging of seizures in vivo, Schwartz and Bonhoeffer *(100)* observed a clear change in reflectance of light associated with each IIS (Fig. 3). As the IIS developed, and its amplitude increased in size, the area, and magnitude of the change in reflectance also increased. Figure 3 shows blank-divided maps of an IIS focus developing in ferret visual cortex. A clear change in reflectance of light can be seen after each IIS. Note that the IIS is seen in the local f.p. but not in the adjacent ECoG. Although the large amplitude of the signal makes imaging a single IIS possible, by averaging over multiple spikes, with spike-triggered image division, the signal-to-noise ratio is improved and time-course of the optical signal is apparent (Fig. 4). The optical signal begins within 500 ms after the IIS and peaks at 1 s (Fig. 4). These studies provoked the following questions, which we explored in the rat. First, if the signal is

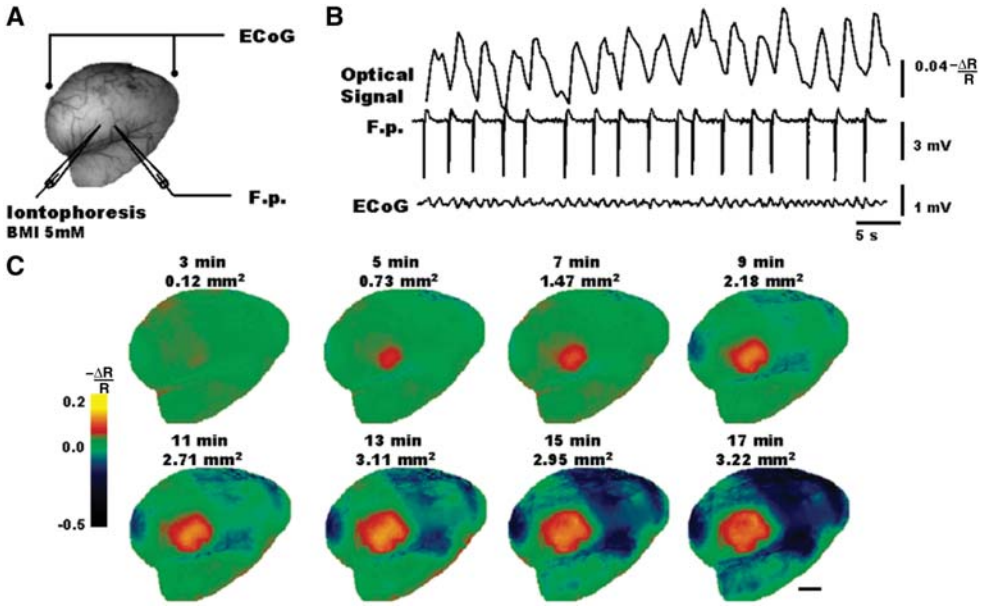

Fig. 3. (A) Simultaneous optical signal, f.p., and ECoG recording show that **(B)** each IIS has a spatially discrete optical correlate. Note that (A) the ECoG, located beyond the limits of the optical signal**, (B)** does not record the interictal events supporting the conclusion that the optical signal indicates the spatial limits of the electrophysiological event. **(C)** BD maps, each averaged over 1 min of recording (~ 21 spikes). During the earliest, small amplitude IIS, the mean area of the focus for all experiments was 0.12 ± 0.02 mm^2, with a minimum of 0.08 mm^2. The area of the focus then increased in size during the next several minutes and finally stabilized at a mean size of 2.84 ± 1.59 mm^2, corresponding with an increase in the amplitude of the f.p. spike. The area of the IIS was derived from the BD maps by thresholding to a pixel value one standard deviation above the pixel values from the area of the focus during control conditions. Notice that the inverted optical signal in the surrounding cortex also increases in intensity and area as the focus develops. Scale bar, 1 mm. (Reprinted with the permission of *Nature Medicine*.)

apparent as early as 500 ms after the IIS, with faster imaging it might be visible even sooner. This would be unusual because the IOS is thought to be a slow signal, as demonstrated in the functional architecture studies. Perhaps in epilepsy, the signal is more rapid? Second, these ferret studies were only performed at one wavelength and the relationship between the wavelength of incident light and epileptiform events had not been explored.

2.2.5. Multiwavelength Imaging in the Rat

Figure 5 demonstrates each individual frame recorded at 10 Hz (100 ms/frame) using spike-triggered image division in rat neocortex at four different wavelengths in the same animal. What is immediately apparent is that the change in reflectance occurs as early as 100 ms after the IIS, regardless of the wavelength recorded. At 546 nm, the tissue darkening in the focus is not seen in the blood vessels, and it takes longer to evolve and appears to spread more widely. An inverted signal is appreciated in the surrounding cortex. At higher wavelengths, the darkening is more focal and there is an inverted signal in the draining veins as well as the surrounding cortex. Also, at higher wavelengths, the signal in the focus develops and dissipates more rapidly. Figure 6 is a graphical representation of the amplitude of the change in light reflectance in the focus and surround as well as the extent of spread of the optical signal recorded at each wavelength. As demonstrated in Fig. 6A, the amplitude of reflectance change in the focus is greatest at 546 nm (0.4%; $n = 7$ rats) and least at 700 nm (0.05%; $n = 9$ rats). When the data are normalized to amplitude, it is clear that the signal increases earlier and more quickly at higher wavelengths (Fig. 6B). A statistically significant change in light reflectance (paired t-test, $p < 0.05$) is observed as early as 100 ms for four rats at 546 nm, eight rats at 605 nm, seven rats at 630 nm, and five rats at 700 nm (Fig. 6C). Likewise, the peak of the reflectance change occurred 1–2 s after the IIS for 605 nm, 630 nm, and 700 nm and 2–3 s after the IIS for 546 nm.

The amplitude and latency of the inverted optical signal in the surround, on the other hand, was similar at different wavelengths (Fig. 6D), which can be seen even when normalized to the maximal amplitude of the inverted signal (Fig. 6E). This inverted signal peaked 1–2 s after the IIS for all wavelengths but also was recorded as early as 100 ms after the IIS. A statistically

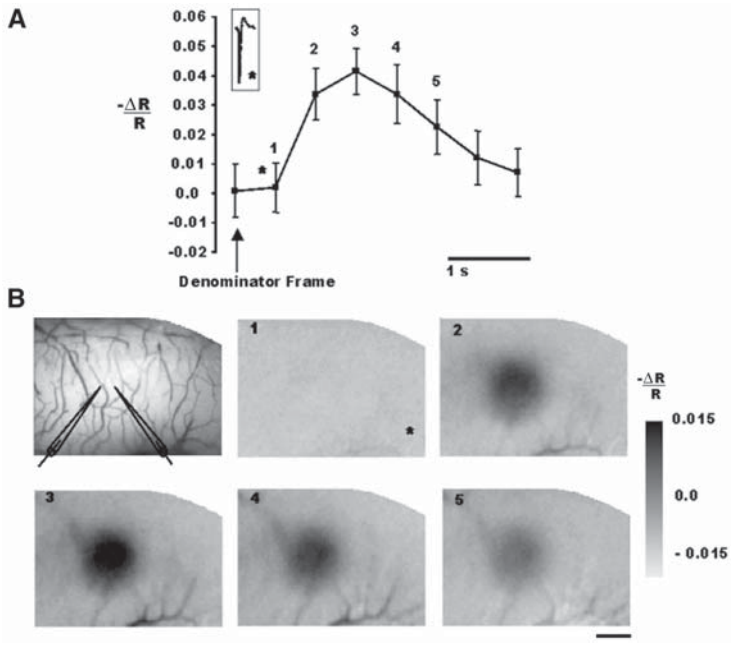

Fig. 4. (**A**) The change in reflectance (-AR/R) as a function of time for the 0.5 s before and 3 s after each IIS is determined with spike triggered image division. The error bars show standard deviation over 116 different spikes. The asterisk indicates the time of occurrence of the IIS. The numbers in (A) correspond to the numbers in the panels of (**B**). The top left panel in (B) shows the location of the electrodes and the blood vessel configuration. Subsequent images show spike-triggered epilepsy maps obtained by dividing each camera frame after the spike by the frame prior to the spike (the "denominator frame"). Divided images are averaged more than 116 spikes. Averaging increases signal-to-noise ratio, though maps can often be seen from a single interictal spike. Scale bar in (B) indicates 1 mm. (Reprinted with the permission of *Nature Medicine*.)

significant change in reflectance in the surround (paired *t*-test, $p < 0.05$) was observed at 100 ms for three rats at 546 nm, six rats at 605 nm, five rats at 630 nm, and two rats at 700 nm (Fig. 6F).

Although in Fig. 5 the change in reflectance of light appears more diffuse at 546 nm and more focal with increasing wavelength, this was not always the case. Figure 6G demonstrates the average area of spread of the change in reflectance in the focus in all animals as a function of time. Although the IOS signal spreads more rapidly at higher wavelengths, as seen in the steeper slope of the curves at 605, 630, and 700 nm, the maximal area (peak) is not significantly different between 546, 605. and 630 nm when averaged among animals (analysis of variance [ANOVA]). The optical signal recorded at 700 nm, however, was clearly more focal than the other wavelengths.

2.2.6. IOS of a Mirror Focus

In several animal experimental models of epilepsy, mirror foci have been described in which an independent epileptic focus develops in a homotopic location in the contralateral hemisphere. Although not described in humans, the etiology likely depends on cross-callosal kindling. In acute models of epilepsy, rapid cross-callosal spread of epileptiform events has been described *(133,134)*. Schwartz and Bonhoeffer *(100)* investigated this phenomenon optically. Using acute focal disinhibition with BMI iontophoresis in ferret somatosensory cortex, the contralateral homotopic area of cortex was imaged and spike-triggered image division was performed based on the timing of the IIS that occurred contralateral to the imaging. Figure 7 shows the results of their experiments. A small epileptic focus could be seen optically in the cortex contralateral to the iontophoresis. Contralateral hemisphere maps, triggered to ipsilateral spikes, showed a clear increase in the optical signal during the first 0.5–1 s, with an average amplitude of $0.4 \pm 0.18\%$ (Fig. 7). As expected from single-unit recordings in homotopic foci *(133,134)*, the optical signal was smaller and slightly more delayed than the signal recorded ipsilateral to a focus. Nevertheless a clear, well-circumscribed focus could be seen, demonstrating that it is possible to visualize epileptic events and detect a focus even if it is comparatively weak and not directly caused by epileptogenic agents.

2.3. IOS OF ICTAL EVENTS

As described in Subheading 2.1.1.2, the 4-AP model is a particularly useful acute model of ictal events for examining the initiation, spread and offset of seizures as well as the rela-

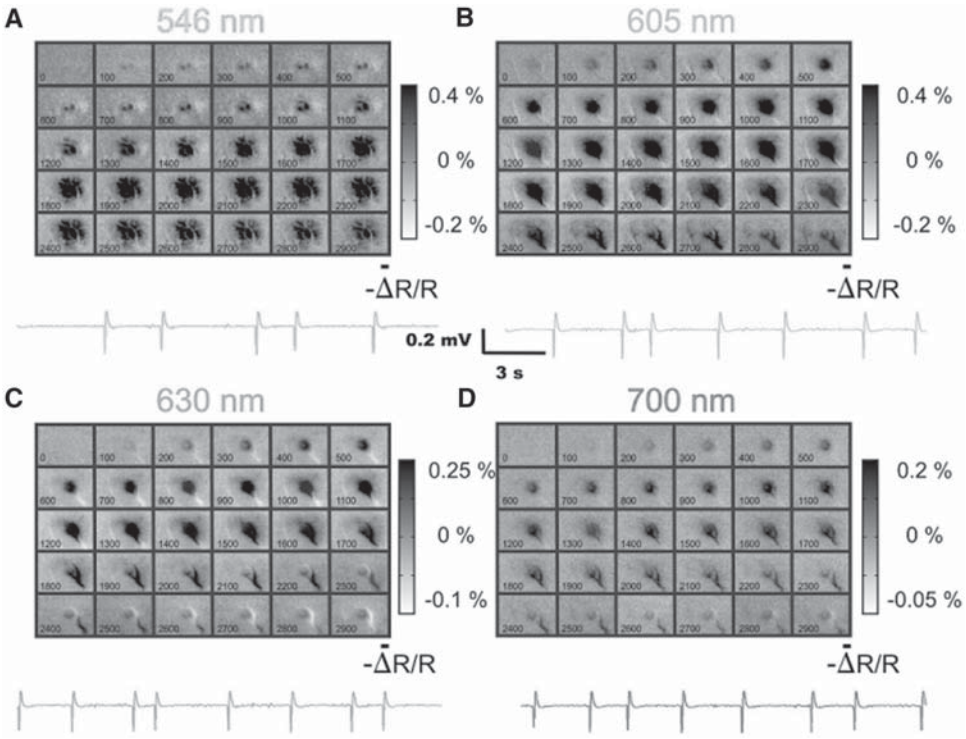

Fig. 5. Multiwavelength fast imaging of IIS. Averaging multiple spikes (100–200) with spike triggered image division at **(A)** 546 ± 10 nm, **(B)** 605 ± 10 nm, **(C)** 630 ± 10 nm, and **(D)** 700 ± 10 nm demonstrate that the intrinsic signal change is evident within 100 ms of the IIS. Note that although there is more blood vessel artifact at higher wavelengths, the intrinsic signal change also appears to be more focal. Draining veins have an early inverted signal higher wavelengths. Examples of IIS field potential recordings are shown at the bottom of each panel. The number at the bottom left of each image indicates the time after the spike occurrence, in units of milliseconds. Scale bar, 1 mm.

tionship between the optical recording at different wavelengths and surface electrophysiological recording of horizontally propagating seizures. Once again, it was initially not clear if the IOS had sufficient temporal resolution to image the horizontal spread of a seizure and whether the ictal onset zone (site of initiation) could be determined prior to lateral propagation.

2.3.1. Methods

The animal preparation and surgical technique are identical to the induction of IIS, except that a glass micropipette filled with a solution of 25 m*M* 4-AP and attached to a Nanoject II oocyte injector (Drummond Scientific, Broomall PA) was positioned less than 1 mm from the field potential electrode. Electrographic seizures were induced by the injection of 0.5 µL of 4-AP (25 m*M* in 1% NaCl) into cortical layers II-III in increments of 50 nL. Once seizures were initiated, they were often stereotypical in form (though exhibiting several different onset morphologies, as discussed below), but varied in duration between animals, from 60 to 300 s. The seizures occurred periodically at intervals of 5–20 min for up to 3 h.

2.3.2. IOS Imaging in Ferret Neocortex

Schwartz and Bonhoeffer *(100)* optically recorded the spread of a 4-AP seizure through ferret visual cortex. They reported that with a frame rate of 2 Hz, at 707 nm, the site of initiation could be localized to a region as small as 1 mm^2 (Fig. 8; ref. *100*). This finding is significant because successful surgery for epilepsy often requires the identification of the ictal onset zone, which must be removed to eliminate seizures *(135)*. Because the rate of horizontal propagation was relatively slow, the IOS appears to be an excellent technique to map seizure propagation. The change in reflectance is almost ten times larger for seizures (~50%) than for the IIS, so no signal averaging is required. In fact, given the variability in the morphology of each individual ictal event, signal averaging would eliminate any inter-seizure variability. Technically, one can divide all

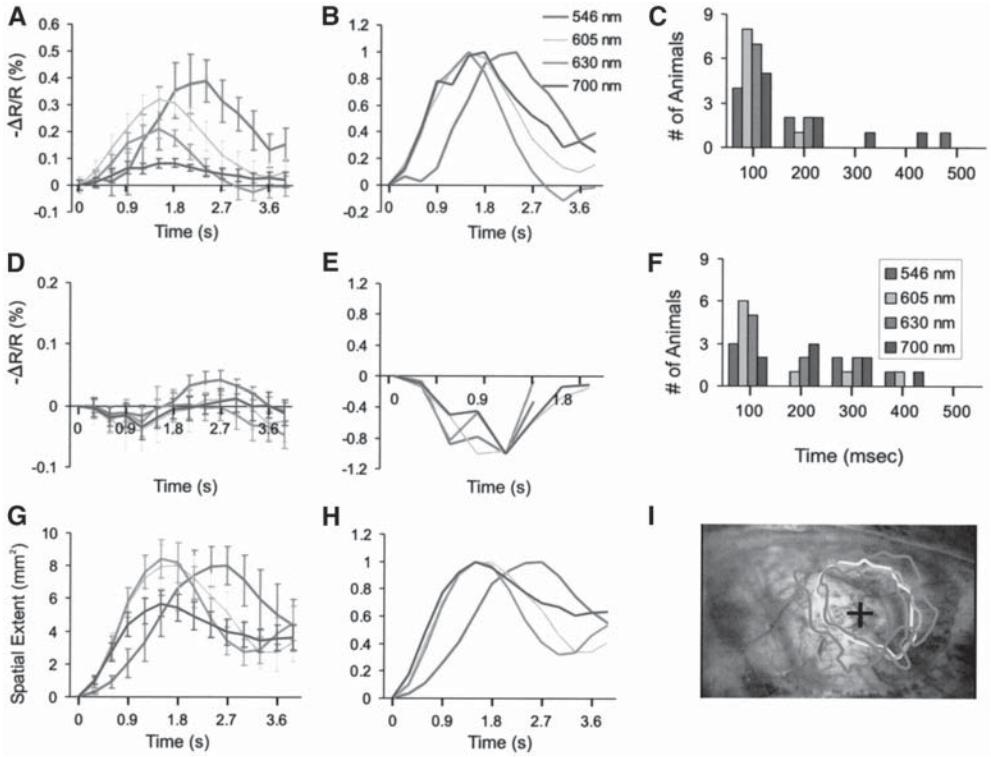

Fig. 6. **(A)** Percent change in reflection of light in the focus as a function of time and wavelength after each IIS. The amplitude of the IOS is clearly greatest when recorded at 546 nm, followed by 605 nm, 630 nm. and 700 nm. **(B)** Data are normalized to the maximum change in reflectance to show that the rise in the signal is fastest at higher wavelengths. **(C)** The earliest statistically significant change in reflectance of light was seen at 100 ms regardless of the wavelength. **(D)** Percent change in reflection of light from the surround as a function of time and wavelength following each IIS. An inhibitory signal is seen in all wavelengths and the amplitude of this inverted IOS is equivalent, regardless of wavelength. **(E)** Data are normalized to the maximum negative change in reflectance to show that temporally there is no wavelength dependence in this signal. **(F)** The earliest statistically significant inverted change in reflectance of light in the surround was seen at 100 ms, regardless of the wavelength. However, in some experiments this negative signal occurred later than the positive signal in the focus. **(G)** The extent of spread (area) of the change in reflectance in the focus over time is less wavelength-dependent. Although the maximal area was achieved earlier at 605 and 630 nm and the rate of lateral spread was faster, the maximal area of spread was similar to 546 nm. At 700 nm, the area of spread was clearly smaller. **(H)** Normalization to the maximal area shows the slower propagation at 546 nm. These data were averaged over multiple animals. **(I)** Thresholding the maximal area of spread in one animal, however, reveals that in this animal, the signal at 546 clearly propagates further than at other wavelengths. *See* color version on Companion CD.

images acquired during the seizure by a "blank" image taken before the seizure onset, generating a "movie" of the seizure (Fig. 8). Schwartz and Bonhoeffer (2001) also noted a region of inverted optical signal surrounding the evolving seizure that disappeared as the seizure spread horizontally. Whether this inverted signal truly represents neuronal inhibition or merely shunting of oxygenated blood to the more active focus is still not clear, although it will be examined in more detail below.

2.3.3. Multiwavelength IOS Imaging of Acute Seizures in Rat Neocortex

To investigate the relationship between the electrophysiology and the IOS signal in the acute seizure model, we imaged 67 seizures in 6 rats at several wavelengths. As with the IIS, the largest amplitude of IOS from the seizure was recorded at lower wavelengths. The average (S.E.) maximal values of –AR/R (%) were 13.70 ± 2.06% at 546 nm (21 seizures in 6 rats), 4.97 ±

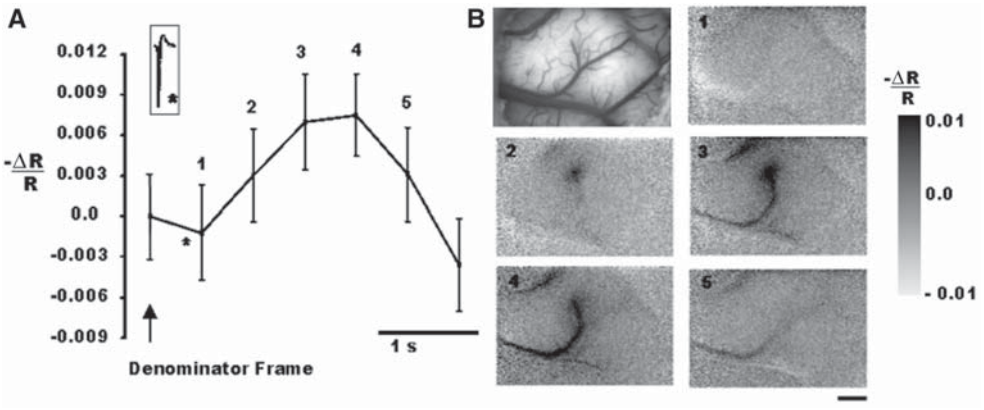

Fig. 7. (A) Secondary, homotopic focus epilepsy maps from the contralateral hemisphere were obtained by triggering the image division to the timing of the spikes in the ipsilateral hemisphere and averaging over multiple spikes. *Y*-axis shows-(R/R as a function of time for the 0.5 s before and 3.5 s after each spike. Error bars (± SD) were calculated from 142 consecutive spikes. (*) refers to the time of the spike and the numbers refer to the images in (B). **(B)** ST epilepsy maps are obtained by dividing each frame after the spike by the frame prior to the spike (denominator frame) and averaging over 142 spikes. The focus is well localized and appears prior to the signal from the blood vessels. Scale bar, 1 mm. (Reprinted with permission from *Nature Medicine*.)

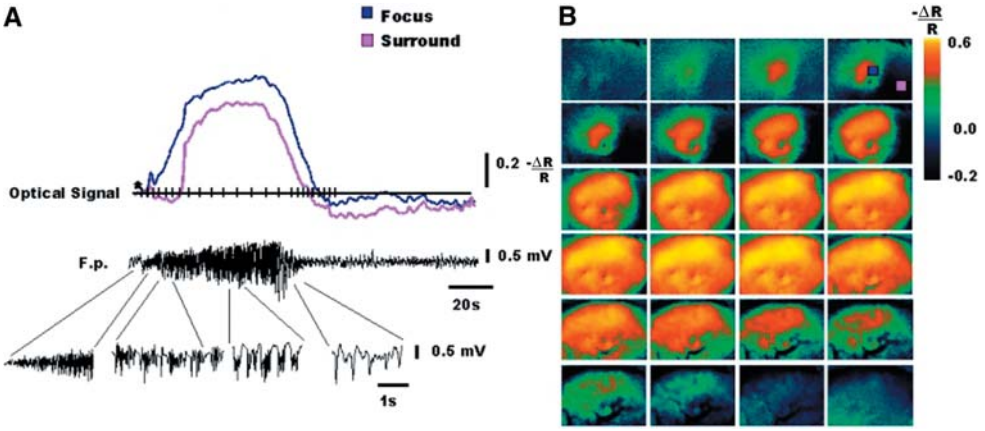

Fig. 8. (A) Optical signal from the focus (blue) and surround (pink) during an ictal event induced by focal application of 4-AP in ferret cortex. Ictal events last 40–80 s with interictal periods of 2–4 min. Each image is generated by dividing a single frame by a denominator frame that occurs prior to the event. (*) refers to the time of the denominator frame for the images in (B). The signal in the surround shows transient inhibition until the event propagates past. **(B)** The timing of each image corresponds with the tickmarks in (A). Images were chosen to show the onset and offset of the ictal event. The dimples in the signal represent the locations of the two micropipettes. Scale bars, 1 mm. (Reprinted with permission from *Nature Medicine*.)

0.79% at 605 nm (15 seizures in 6 rats), 3.80 ± 0.71% at 630 nm (15 seizures in 6 rats), and 1.90 ± 0.38 % at 700 nm (16 seizures in 5 rats; ANOVA, $p < 0.0001$; post-hoc Student-Neumann-Keuls (SNK) test significant for 546 nm vs 700 nm, 630 nm and 605). As discussed earlier, the signal at 546 nm is near the isosbestic wavelength of hemoglobin and is more sensitive to blood volume. Wavelengths from 600 to 650 nm image oxy/deoxyhemoglobin and >660 nm include signal from light scattering. It is not clear why the amplitude of the ictal signal is less in the rat than in the ferret. Perhaps imaging though the intact bone and dura in the rat may have attenuated the signal, although the percent change should not be affected.

Figure 9 demonstrates ictal events recorded at three different wavelengths. One can clearly see that each seizure is slightly

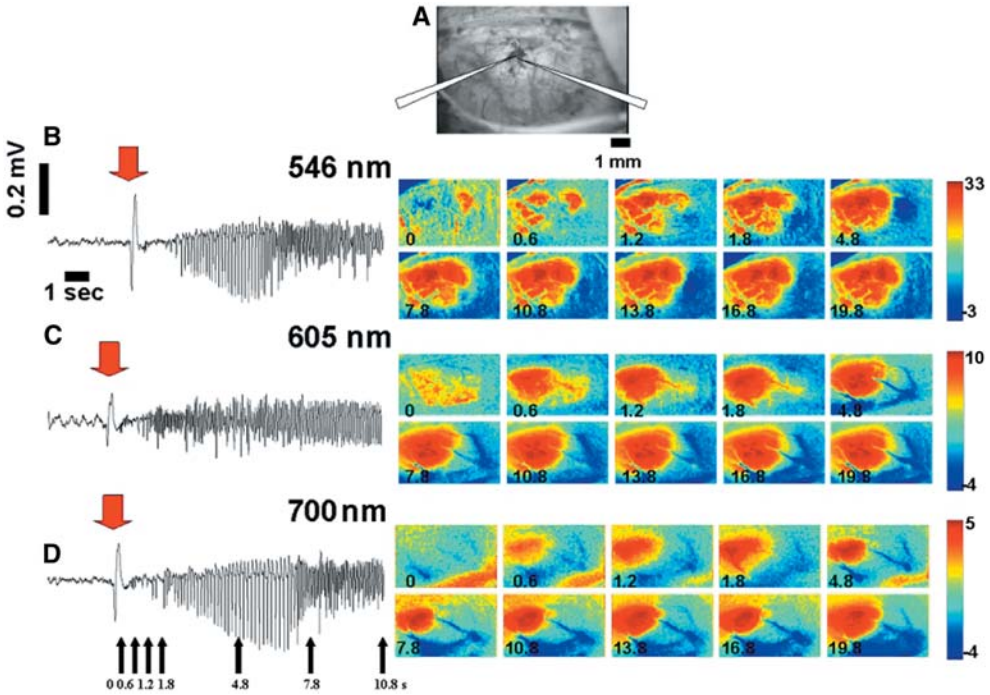

Fig. 9. **(A)** Thin skull 546-nm image or blood vessel pattern with position of f.p. electrode and 4-AP pipette. **(B–D)** The f.p. recording of the seizures is on the left and the corresponding imaging on the right. Each ictal event differs slightly from the others. The timing of the images noted on the image and with black arrows under (B). The red arrow indicates the onset of the seizure and the "denominator frame." Recordings were made at 546 nm (B), 605 nm (C), and 700 nm (D). Scale bar units show –AR/R (%).

different electrographically. In the example shown in Fig. 9, the optical signal at 546 nm appears to be less focal than at higher wavelengths. However, using the thresholding technique described in Subheading 2.2.3., on average, there was no statistical difference in the maximal area of spread comparing seizures imaged at 546 nm (20 seizures in 6 rats), 605 nm (15 seizures in 6 rats), 630 nm (15 seizures in 6 rats), and 700 nm (15 seizures in 6 rats). The inverted optical signal also was apparent at all four wavelengths. The average maximal (S.E.) inverted optical signal in the surround (here described as –AR/R, so that an increase in reflectance is a negative number) was –4.56 ± 0.85% at 546 nm (21 seizures in 6 rats), –9.62 ± 1.51% at 605 nm (15 seizures in 6 rats), –7.45 ± 1.39 % at 630 nm (15 seizures in 6 rats), and –3.98 ± 0.56 % at 700 nm (16 seizures in 5 rats) (ANOVA, p value of 0.0019). A post-hoc SNK test showed that the increase in reflectance at 605 was significantly greater than that at both 700 and 546 nm ($p < 0.01$).

2.3.4. Electrographic Variability and IOS Variability

In human epilepsy, two common electrographic patterns of ictal onset have been defined, originally in medial temporal lobe recordings from humans, but also found in the neocortex: (1) periodic spiking and (2) low-voltage fast activity (LVFA; refs. *136–140*). Periodic spiking involves high amplitude repetitive spike-and-wave events that can occur in low (1–2 Hz) or at higher frequencies (10–20 Hz) in the few seconds before or immediately at seizure onset, which may then evolve into LVFA or continue as periodic spiking *(139,140)*. Periodic spiking is characterized by single-unit burst and suppression patterns. Corresponding in time to the "spike" and the "wave," respectively, that are less likely to propagate or secondarily generalize, and resemble recurrent IIS *(136–138)*. This type of ictal onset has been correlated with an increase in inhibitory tone based on single unit recordings *in situ* in human hippocampus *(77,136)*, although contrary data have been demonstrated in resected hippocampal specimens *(141)*. LVFA, also called the "recruiting rhythm," on the other hand, is believed to represent periods of disinhibition, based on in situ human hippocampal single-unit recordings, in which the field oscillations occur at much higher frequencies (>30 Hz) compared with during periodic spiking *(136–139,141)*. This type of activity is though to propagate more readily to adjacent brain and become symptomatic *(137,138)*.

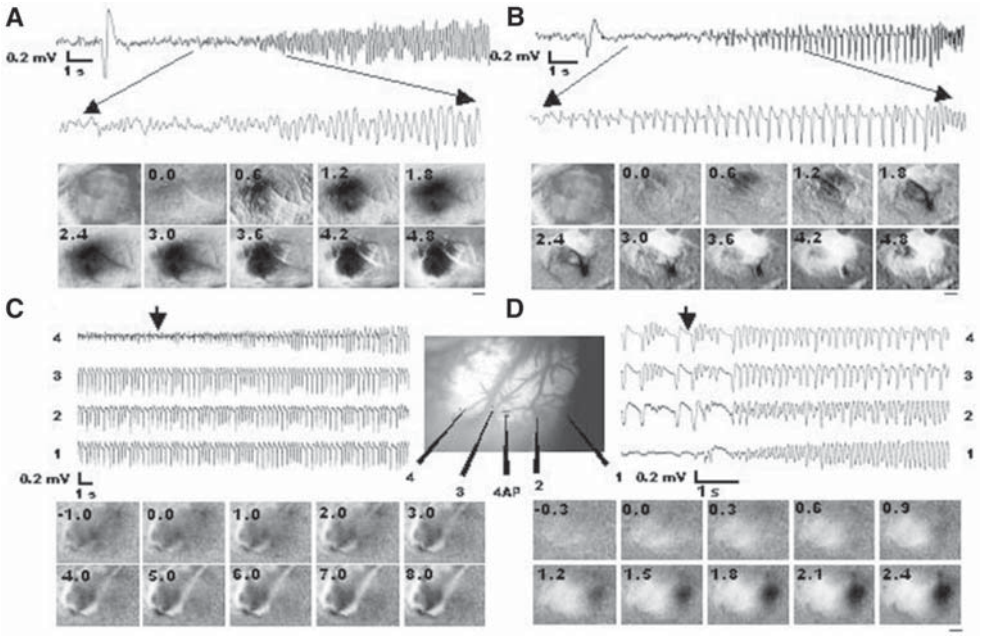

Fig. 10. Most acute 4-AP-induced seizures start with a single large spike followed by attenuation. Then, either **(A)** LVFA or **(B)** periodic spiking ensues. Optical imaging demonstrates that (A) LVFA causes a more rapid spread with less surrounding inhibition compared with (B) periodic spiking. Using a multicontact linear array of electrodes, we can image seizures originating sequentially at several different sites as inhibitory activity shifts accordingly. In **(C)** the onset is at electrode 4 and in **(D)** the onset is at electrode 1. This complex interaction is not apparent from the electrophysiology. The number at the top left of each image indicates the time after the electrographically defined seizure onset, in units of seconds. Scale bar, 1 mm. Seizures shown here are imaged with incident light of wavelengths 605 nm.

With the 4-AP model, seizures generally begin with a large spike followed either by LVFA (Fig. 10A) or periodic spiking (Fig. 10B). Each seizure is slightly different and sometimes the initial spike is absent and the length of time spent in either LVFA or periodic spiking is quite variable. Accordingly, the optical signal is variable. Even when imaging at a single wavelength, the dynamic relationship between excitation and inhibition, the focus and the surround, is quite evident. In Fig. 10A, the seizure begins with LVFA and the optical signal spreads rapidly with almost no negative signal in the surround (Fig. 10C). In contrast, the seizure in Fig. 10B begins with periodic spiking and the optical signal spreads less rapidly and there is a large inverted signal (Fig. 10D). This raises the tantalizing possibility that the optical signal is quite sensitive to excitatory and inhibitory activity and may show us the dynamic topography of this relationship, providing a map of the variability of the electrographic event.

Further support for this finding comes from simultaneous multicontact f.p. recordings and IOS imaging of ictal events. In Fig. 10C, we see a seizure developing in one area of cortex, while another seizure is occurring in a separate area of cortex. In Fig. 10D, a seizure begins within yet another area of the cortex. The corresponding optical images accurately demonstrate the spatial specificity of each of these events and the shifting foci. The topography of each set of optical maps is clearly different as is the electrographic recording. Each method provides complementary yet different information about the same event.

2.3.5. Ictal Onset Versus Offset

In human epilepsy, the area of ictal termination is not always identical to the area of initiation. The significance of this phenomenon is not well understood, but it may have prognostic significance for successful surgical treatment *(142)*. Several theories exist to explain why and how seizures terminate. One possibility is a return of inhibitory function, which eventually terminates the ictal discharge *(137,138)*. As seizures terminate, neuronal synchronization returns *(143)*. Other theories of seizure termination involve hyperpolarization via the Na-K pump *(144)*, rundown of transmitter release *(145)*, pacemaker failure *(129)*, or a large depolarizing shift, not involving neuronal inhibition, similar to spreading depression *(146)*.

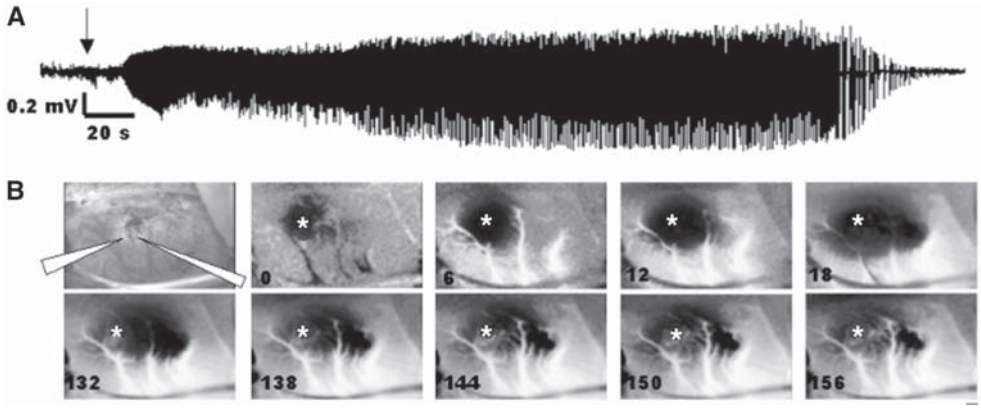

Fig. 11. (A) Field potential recording from 4-AP induced seizure show that ictal onsets appear electrographically different than offsets but the spatial extent of this difference is not known. **(B)** The intrinsic signals show that the area of onset (asterisk) is spatially not co-localized with the area of offset (*see* last image). The numbers in images correspond to the time after the onset (arrow). Scale bar, 1 mm. *See* color version on Companion CD.

In acute 4-AP seizures, we have observed that the location of seizure onset (determined as the centroid of the darkened region at the time of its first statistically significant rise above baseline, with the areal extent of the region determined by the thresholding method described above) often differs from the location of offset. This is illustrated in ferret cortex in Fig. 8 and in rat cortex in Fig. 11. We clearly do not see any evidence of spreading depression, which causes a large IOS change, and thus our findings contradict that theory. We also do not see an inverted signal that terminates the seizure, so a rise in inhibition may also not be critical. Regardless of the precise mechanism of seizure termination, IOS imaging is an ideal technique for investigating the relationship between ictal onset and offset zones.

2.4. IOS IMAGING OF THE RELATIONSHIP BETWEEN EPILEPTIFORM EVENTS AND FUNCTIONAL ARCHITECTURE

One of the best clinical examples of the interaction between functional brain architecture and epilepsy is "pattern-sensitive epilepsy", in which epileptic events are triggered by patterned visual stimuli *(147,148)*. Another example is the periodicity of horizontal spread of epileptic events, thought to reflect the columnar architecture of the cortex and the anisotropy of long-range horizontal connections *(66,67)*. To investigate this relationship, Schwartz *(27)* performed simultaneous IOS recording of an interictal focus as well as orientation and spatial frequency columns in ferret visual cortex. Depending on which column was injected with the epileptogenic agent, patterned visual stimuli of a particular orientation and spatial frequency could trigger each IIS *(27)*. Within the focus, the orientation and spatial frequency columns were severely distorted. In the adjacent surrounding cortex, however, the columnar architecture was not only preserved but could be easily mapped with IOS. This implies that in spite of the altered cerebral hemodynamics caused by the epileptic focus, the IOS was still accurate at mapping functional architecture within a millimeter of the focus (Fig. 12). This may prove very important for human mapping of functional architecture in patients with epilepsy adjacent to eloquent cortex.

2.5. ANIMAL MODELS OF CHRONIC EPILEPSY

Chronic neocortical foci are thought to represent a model of epileptogenesis that more closely approximates the situation in the human. Seizures develop during the course of days to months rather than seconds to minutes and last from weeks to years. Although the precise mechanism of neocortical epileptogenesis in chronic models is unknown, the etiology is thought to be multifactorial with evidence for alterations in local disinhibition *(149)*, intrinsic membrane properties favoring hyperexcitability in pyramidal neurons *(150)*, axonal sprouting in layer 5 leading to enhanced recurrent excitation *(151)*, glial regulation of extracellular potassium *(152)*, and neurotransmitter-specific neurons or receptors *(153)*. Chronic models are generally produced with the subpial injection of metal compounds such as aluminum hydroxide, cobalt, tungsten, or iron into somatosensory cortex *(109,154)*. Chronic foci tend to be more diffuse than acute foci and may produce multiple areas of epileptogenesis *(91,155)*. Surface recordings show that population spikes rarely reach 1 mV compared with spikes of 3–5 mV in acute foci *(62,63,91,155)*. The lower amplitude of interictal spikes reflects the smaller percentage of cells that participate in each interictal event *(90,91,155,156)*. Electrophysiologic mapping of chronic foci with single cell recordings has demonstrated that anywhere from 10% to 50% of the sampled populations exhibit spontaneous bursting activity simultaneous with surface potentials *(90,91,118,155,157)*. There is also a variable and inconsistent correlation between

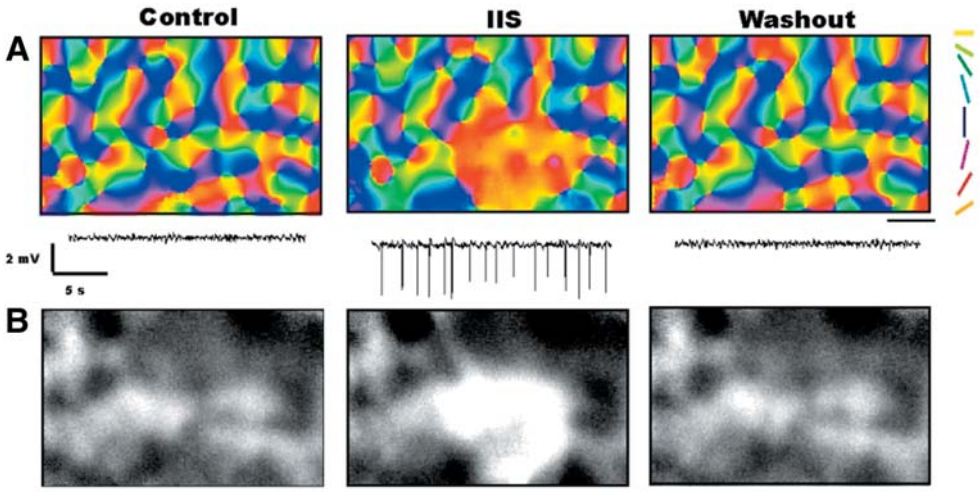

Fig. 12. (A) Angle map generated before, during and after iontophoresis of BMI into ferret cerebral cortex elicits IISs. The intrinsic signal within the focus is distorted by the occurrence of the IIS. The intrinsic signal from the surrounding cortex, however, is unaltered. The dominant yellow color in the focus indicates that 0º stimuli were more likely to trigger spikes than other orientations. Sample of the f.p. recording simultaneous with the imaging is shown under (B). Scale bar, 1 mm. **(B)** Spatial frequency maps from the same animal demonstrate that low-spatial frequency stimuli are more likely to trigger IIS than high-spatial frequency stimuli and that these maps are also distorted within the IIS focus but preserved in the surrounding brain. (Reprinted with permission from *Cerebral Cortex*.) *See* color version on Compannion CD.

surface potentials and single neuron action potentials indicating that the size of the epileptic aggregate varies from burst to burst and separate discharges begin at different sites *(90, 91,119,155)*. Electrophysiologic studies in chronic foci have also failed to report a significant amount of cellular inhibition from the neurons in the surrounding cortex, although few of these studies have specifically examined this issue *(91, 120,155)*. It has been hypothesized that the diffuse, less intense chronic focus does not strongly recruit recurrent inhibitory circuitry *(91,155)*. Overall, chronic models tend to approximate findings in chronic human epilepsy and provide a better model for investigations into epileptogenesis. We have concentrated on two models of chronic epileptogenesis in our IOS studies in the rat.

2.5.1. The $FeCl_2$ Model

Subpial microliter injections of iron salts are a reliable model of chronic interictal and ictal epileptogenesis which are particularly effective in rodents *(158–161)*. This model is particularly relevant to post-traumatic or post-hemorrhagic human epilepsy that emerges after the extravasation of blood and deposition of iron into the neuropil. The mechanism of action is not clear but may involve the free radical intermediates of oxygen and peroxidative stress on cell components as well as inhibition of Na^+/K^+ adenosine triphosphatase *(162)*. Isolated spikes appear in 90% of animals after 72 h and stabilize at 30 d with a frequency of three spikes/min *(158–161)*. Spike-and-wave complexes accompanied by behavioral manifestation appear in 75–100% of animals starting at 30 d and stabilize at 90 d *(159,161,163)*. Both types of events remain stable for up to 12 mo. Epileptiform activity contralateral to the injection has also been reported *(163)*. Histologic analysis of the resulting lesion reveals hemosiderin-laden macrophages, fibroblasts, gliosis, neuronal cell loss, and a decrease in the number of dendritic spines *(159,164)*. These findings are reminiscent of those found both in aluminum hydroxide-induced animal models and human epilepsy *(165,166)*. In vivo microdialysis reveals similar changes in extracellular amino acids as in chronic human epilepsy *(163)*.

2.5.2. The Tetanus Toxin Model

Injection of tetanus toxin to induce chronic epilepsy in the rat has been studied both in the hippocampus and in the neocortex *(167–173)*. Tetanus toxin acts by blocking exocytosis preferentially in inhibitory interneurons, thereby decreasing GABAergic inhibition *(174–177)*. Rapid but patchy spreading to adjacent and contralateral cortex occurs though axonal and transsynaptic mechanisms *(178,179)*. Injection of nanogram quantities into the cortex of the rat leads to spontaneous interictal events within 3–5 d in almost 100% of the animals at a rate of 0.2–2 spikes/s *(170)*. In the hippocampus, epileptiform events are multifocal, often arising at a distance from the injection site *(171)*. Behavioral seizures have been reported in as many as 92% of injected rats *(180)*. Spontaneous independent events arise in contralateral homotopic cortex occurs several days later. These events last for longer than 7 mo, long after the toxin has been cleared from the tissue given a half-life of only a few days, indicating that long-lasting plastic changes cause chronic epileptogenicity *(181)*. In

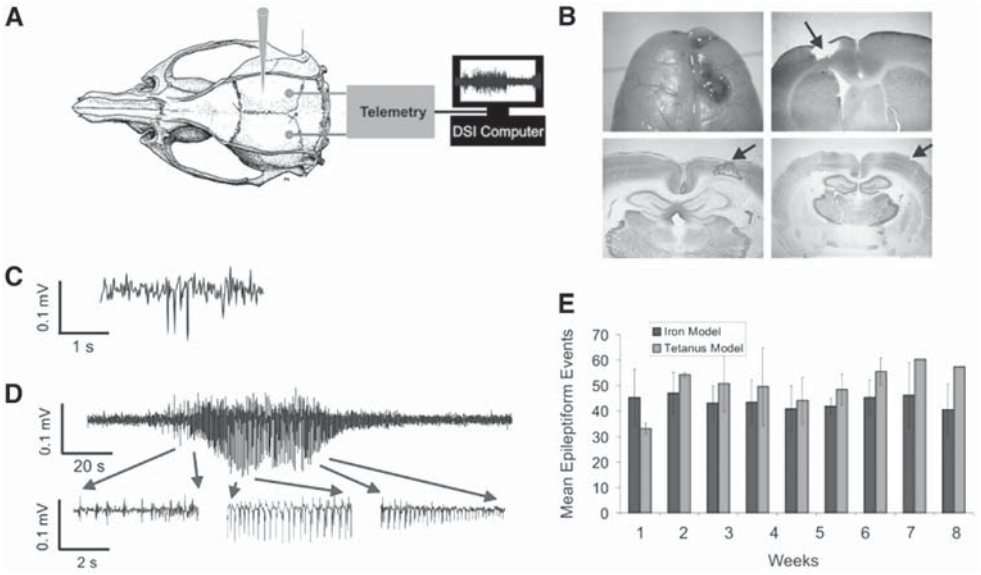

Fig. 13. Using video-EEG monitoring and telemetry **(A),** we can record chronic epileptiform events in rats, which are stable for several months **(E)**. **(B)** Whereas the injection of iron creates a cavitary lesion seen grossly (top left) and with Nissl (top right) and parvalbumin (lower left) staining, tetanus toxin is nonlesional (lower right). Arrows indicate site of injections. Both interictal **(C)** and ictal **(D)** events are recorded during chronic video-EEG monitoring and quantified using custom-written seizure detection algorithms (*see* Section 3.3.). Scale bar, 1 mm. *See* color version on Companion CD.

vitro intracellular recordings reveal a characteristic PDS during field recordings of interictal events *(170)*. Histologically, there is no cell loss or gliosis *(180,182)*.

2.5.3. Methods

Under ketamine/xylazine anesthesia, rats were placed in a stereotactic frame and a small parasagittal skin incision and a trephine hole (0.5 mm in diameter) were made under sterile conditions, 2.5 mm lateral and 1.5 mm rostral to the bregma over the hindpaw sensorimotor cortex. Then, 2.5 µL of 400 m*M* $FeCl_2$ or 50 ng/0.5 µL tetanus toxin was injected 1–2 mm below the surface through the hole using an oocyte injector. Two stainless-steel epidural screw electrodes (0.5 mm in diameter) were implanted into opposite sides of cranial bone, 3 mm lateral and 3 mm rostral to the bregma and 4 mm lateral and 4 mm caudal to the bregma for chronic ECoG recording (Fig. 13A). These electrodes were soldered to the distal wires of a two-lead telemetry system (DSI) and a transmitter was placed under the skin in a pocket between the shoulder blades. The surgical field was irrigated with antibiotic solution and closed. The animals were awakened and placed in a facility for chronic behavioral and video-EEG monitoring for epileptic activity. Signals were digitized onto a PC. Quantification of interictal and ictal events was performed with the use of a custom-made seizure detection algorithms written in MATLAB (The MathWorks, Inc.) The signals were bandpass filtered (3 to 70 Hz) and the signal energy (power of EEG) associated with the EEG is computed. Each peak that crosses a fixed threshold is counted as one seizure. IISs are also counted using a custom made C^{++} program. Animals with consistent interictal and ictal spikes with or without behavioral events (paroxysmal twitching in the musculature contralateral to the epileptogenic agent with or without secondary generalization) were used for further study. These animals were prepared for imaging as in the acute epileptogenesis models.

Rats with chronic epilepsy from iron or tetanus toxin injection occasionally do not have spontaneous seizures while under anesthesia. Events can be triggered by one of two methods. Because the epileptogenic agent is injected into the area of somatosensory cortex corresponding with hindpaw representation, focal peripheral stimulation of the hindpaw with an S48 stimulator (Grass Telefactor, W. Warwick, RI) delivered through an SIU-7 to apply a 1 mA, 5-Hz stimulus of 2-s duration has successfully triggered epileptiform events. Alternatively, one can administer BMI, 1 mg/kg i.p. every 10 min.

Rats were injected with a lethal dose of pentobarbital sodium (120 mg/kg, i.p.) and perfused transcardially with saline followed by 4% paraformaldehyde and 0.1% glutaraldehyde. After removal of the brains, they were postfixed and stored overnight in a 100 m*M* phosphate buffer (pH 7.4) containing 30% sucrose. Serial coronal sections were cut through the injection site of the iron or tetanus

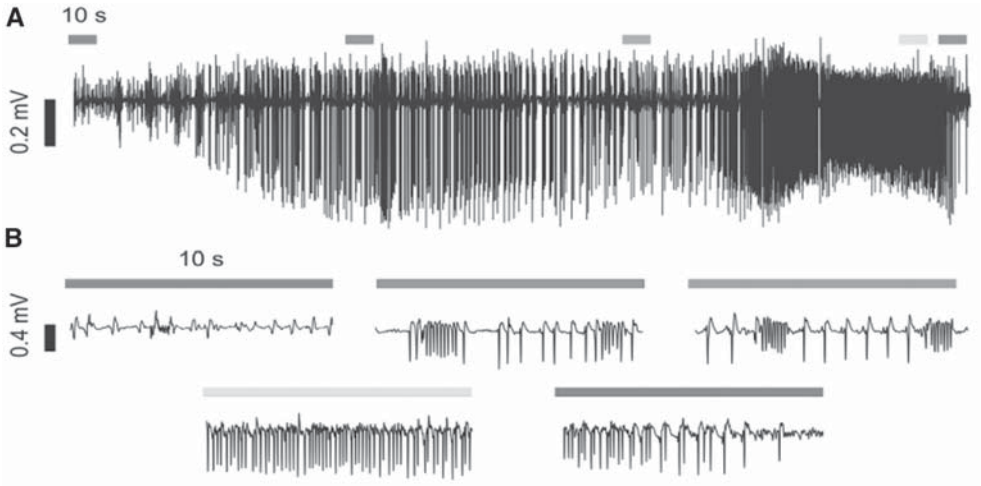

Fig. 14. Interictal spikes and ictal events occur under general anesthesia in chronically epileptic rats. **(A)** Field potential recording from a rat with tetanus-toxin induced epilepsy demonstrates a stereotypical ictal event occurring while under anesthesia. **(B)** Expanded regions from (A) reveal the build-up and diminution of recurrent spike-and-wave activity. *See* color version on Companion CD.

toxin using a freezing microtome (Leica) at 40 μm. Sections were serially stained for Nissl, parvalbumin, glial fibrillary acidic protein, somatostatin, and σ6aminobutyric acid (Fig. 13B).

2.5.4. IOS Imaging of Chronic Neocortical Epilepsy

The iron and tetanus toxin models are not only useful as models of chronic neocortical epilepsy, but also as models of lesional versus nonlesional epilepsy. Whereas iron injection creates a cavitary lesion in the brain, the tetanus toxin injection does not disrupt the cortical architecture (Fig. 13B). Despite these histologic differences, both models generate a stable epileptic focus exhibiting both spontaneous IIS (Fig. 13C) and ictal events (Fig 13D) that are consistent in frequency over time (Fig. 13E). Even under general anesthesia, these animals exhibit epileptiform events suitable for imaging (Fig. 14).

IOS imaging of IIS and ictal events was performed in both models to map the areas of epileptic activity with respect to the injection site of the epileptogenic agent. Our hypothesis was that IIS and ictal onsets would arise from different areas within a single animal, demonstrating a shifting focus, and that the dynamic interaction between excitation and inhibition responsible for this variability would be apparent in the IOS maps. Figure 15A demonstrates the relative locations of the ictal onsets, ictal offsets, and IISs in a single animal relative to the architecture of the pial blood vessels seen though the thinned skull. The IOS clearly demonstrates that each epileptiform event arises from a different area of cortex adjacent to the lesion, with an inter-event distance as far as 8 mm. Figure 15B shows the electrophysiology and IOS imaging at 546 nm during single ictal event. As in the 4-AP acute seizure, chronic seizures also manifest periodic spiking and fast activity. In this example, the seizure begins with periodic spike-and-wave activity and the IOS demonstrates a darkened focus contained by a ring of inverted optical signal in the surrounding cortex. As the ictal event progresses to faster activity with no intervening "wave," the inverted activity disappears and the darkening in the focus spreads to adjacent cortex. These experiments provide further evidence that the IOS can reveal complementary data about excitation and inhibition that form the basis of the electrographic data recorded with field electrodes. Future experiments with multiple single-unit and field recordings and voltage-sensitive dyes will help us understand the complex relationship between imaging and electrophysiology.

3. HUMAN IMAGING IN THE OPERATING ROOM

3.1. BACKGROUND

The past few years have seen a rapid growth in brain imaging techniques used in a clinical setting. Chief among these have been techniques such as fMRI and positron emission tomography. The fast time course and high spatial resolution observed in laboratory studies using the IOS quickly sparked interest in applying this technique to intraoperative imaging. Although high-resolution IOS requires an exposed cortex, which makes it more invasive than other imaging techniques, its promise of extremely high spatial resolution offers an attractive alternative for intraoperative cortical mapping in humans, and also, as we shall see below, the possibility of localizing interictal and ictal epileptiform events during epilepsy surgery.

The IOS was first used intraoperatively by MacVicar and colleagues in 1990 *(183)* for the imaging of stimulation-evoked cortical activation. This study was soon followed by that of Haglund et al. *(102)*, who imaged both stimulation-evoked

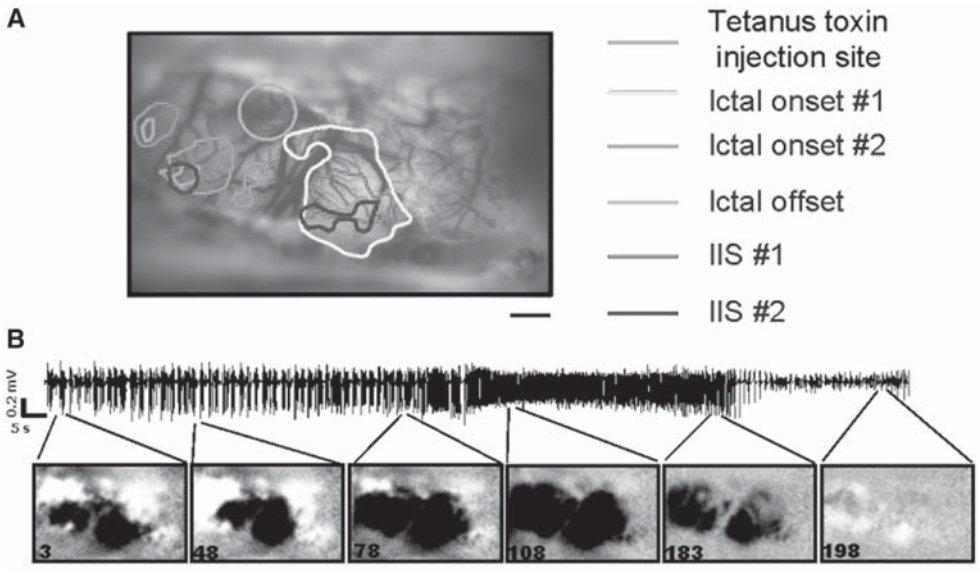

Fig. 15. (A) IOS imaging map of separate ictal onsets, offsets and IISs from the same animal as that illustrated in Fig. 14. Thresholds for area measurements are derived from pixel values 15% above the median of all pixel values. Scale bar, 1 mm. **(B)** The transition from periodic spiking activity to faster spiking in the f.p. is correlated with an increase in the size of the excitatory optical signal and a disappearance of the inverted optical signal in the imaging. The numbers in the images refer to the time(s) when the images were acquired after the onset of the ictal event. *See* color version on Companion CD.

epileptiform afterdischarges and cognitively evoked functional activity such as activation of Wernicke's and Broca's areas during language tasks. A group at UCLA lead by Arthur Toga has published several articles intraoperative human imaging of somatosensory and language cortex *(16,184–189)*. Other groups have also imaged somatosensory cortex, including Shoham and Grinvald *(38)* and Sato et al. *(190)*, who described the ability to image both primary and secondary somatosensory areas.

3.2. TECHNICAL CHALLENGES

Although IOS of human cortex in the operating room is quite feasible, the signal is not as robust as in the laboratory and the spatial resolution is lower due to several technical challenges and large sources of noise *(16,38,102,184,185,189–191)*. The major sources of noise include motion of the cortex induced by heartbeat and respiration, as well as a 0.1 Hz vasomotor signal, each of which change the reflected light signal with a different periodicity *(33,189,192)*. In addition to the time constraints of the operating room, the environment is more difficult to control, resulting in larger fluctuations in ambient light *(102,191)* and anesthesia *(191)*.

Various mechanisms have been developed to compensate for these sources of noise. Image acquisition can be synchronized to the cardiac and respiratory cycles *(184,191)*. The cortex can be stabilized with a glass footplate *(38,102,190)*. Various post-hoc algorithms can also be applied to remove noise from the imaging data. These can include warping algorithms *(102,184)*, or, if a sufficiently long series of images can be obtained, an inverse FFT algorithm can be employed to remove periodic fluctuations from the time course of the signal *(10,33,193)*.

Another difficulty in intraoperative human imaging is the large field of view and the natural curvature of the surface of the human brain. The typical craniotomy is 10–14 cm in diameter. Given the curvature of the brain, keeping the entire surface homogeneously illuminated and in focus would require multiple sources of light and a very large depth of field, which in turn would increase blood vessel artifact, since in the laboratory setting a narrow depth of field permits imaging from a plane below the pial surface and vasculature *(130)*. Various solutions have been implemented such as using a dedicated zoom lens with separate sources of epi-illumination, using the operating microscope lenses and built-in white light illumination with absorption filters or a ring illuminator with filtered incident light. Suspending the camera over the patient's head is also a challenge and investigators have used rigid stands on the floor, attachments to the operating table or the operating microscope itself.

We recorded fluctuations in light reflectance in one pixel over time during an imaging session. Data was sampled at a rate of 1 frame/300 ms during a period of 105 s, an FT was performed and the power spectrum calculated (Fig 17B). The peak indicated by the arrow at left shows the peak for vasomotor

noise (~0.1 Hz); the arrow at the right shows the peak corresponding to the patient's heartbeat (~1 Hz). Methods for eliminating these sources of noise will be discussed.

3.3. METHODS

Patients suitable for intraoperative imaging are undergoing craniotomy for resection of neocortical pathology such as epilepsy, tumors or vascular malformations adjacent to functional cortex. Once in the operating room, their heads are fixed rigidly to the table with a Mayfield headholder (Ohio Medical). General anesthesia is induced with i.v. thiopental, 3-5 mg/kg and i.v. fentanyl, 50–150 μg, in an average adult and maintained with N_2O/O_2 and isoflurane 1%. A nondepolarizing muscle relaxant, Pavulon, 0.1–0.15 mg/kg is given i.v. to facilitate endotracheal intubation. The line of incision is infiltrated with a mixture of equal volumes 1% Lidocaine (with epinephrine 1;100,000). Craniotomy is performed using standard neurosurgical techniques. Once the cortex is exposed, the N_2O/O_2 is discontinued and the patient is maintained on isoflurane 0.2% and supplemental fentanyl 50–150 μg as necessary for the electrical and optical recordings. This combination of anesthetics has been shown to have a minimal effect on the ECoG *(194)*.

In our first experiments (Yale University), we used we reproduced the laboratory setting and imaged a small field of view using a tandem lens arrangement *(*refs. *130*,*190*). The camera was held in place by modifying the Mayfield (Ohio Medical) U-bar that attached to the table and sits over the patient's chest (Fig. 16A). The camera was held by an X,Y,Z-manipulator (Narishige, Japan) and the entire apparatus was placed in a sterile drape. Cortical illumination was achieved with a ring illuminator attached to a DC-regulated power supply and a broadband filter 650 ± 50 nm. A second locking retractor provided another point of fixation between the Mayfield head-holder and the ring-illuminator, which was fixed to the camera lens. In this way, there was minimal relative movement between the cortical surface and the camera lens. Cortical stabilization was achieved with a glass footplate held with the Greenberg retractor system (Fig. 16B). In our later experiments (Weill-Cornell Medical College of Cornell University), we built a camera holder that sat on the floor at the head of the bed and locked to the headholder while suspending the camera over the head on a gross and fine X,Y,Z-manipulator (Fig. 17A). The cortex was illuminated with a ring illuminator on a retractable arm extending down from the camera lens (single 50 mm lens). By lowering the ring illuminator closer to the cortex we increased the intensity of the light and were able to use narrow band filters (± 10 nm). The 50-mm lens increased the field of view to 8 × 8 cm. The cortex was stabilized with a glass footplate.

3.4. INTRAOPERATIVE IOS OF SOMATOSENSORY ARCHITECTURE

We used IOS imaging to investigate somatotopy in the human face area *(195)*. In particular, we wanted to determine the relative cortical location of peri-orbital skin versus skin of the lateral face. Animal studies using microelectrode recordings from Macaque and Cebus monkeys have shown that cortical representation of the peri-orbital skin in Brodmann Area 1 is both rostral and medial to peribuccal skin *(196–198)*. Maps of human face somatotopy generally show peri-orbital skin medial, but not rostral, to lateral face, but these have been generated using cortical stimulation mapping which has a limited spatial resolution *(199–201)*. The field of view using the tandem lens was 14 × 8.7 mm. Three stimulus conditions were used: upper face stimulation, lower face stimulation, and blank. Stimuli consisted of four constant current electrical pulses of 1.5 msec duration with a magnitude of 2.2 mA delivered at 2 Hz through ball electrodes placed below and lateral to the left eye and along the left lower cheek parallel to the lips by an S-88 stimulator (Grass Instruments, Quincy, MA). Each stimulus condition was presented in pseudo-randomized order with a 10- to 15-s interstimulus interval. For each stimulus condition, we collected 10 consecutive 300 ms image frames after stimulus onset and these were stored for subsequent analysis. We collected five blocks of five trials per stimulus.

Stimulation of the upper face produced a focal change in reflectance in a different location than stimulation of the lower face (Fig. 16). Here we demonstrate with high-resolution optical imaging that indeed, in the human, the lateral face is represented both rostral as well as medial to peri-buccal skin *(195)*. We also examined the cortical magnification factor (CMF), which is defined as the area of cortex dedicated to the representation of an area of skin *(202)*. The CMF was calculated from the distance between the electrode contacts on the face (~7 cm) and the distance between the centers of the change in reflectance on the cortical surface (~2.5 mm). The calculated CMF was 0.36 mm per cm (2.5 mm/7 cm) of facial skin. A comparable measurement from the face area of the cynomolgus Macaque is 0.75 mm of cortex per cm of facial skin (cf. Nelson et al., 1980 *[196]*, Fig. 11, distance between center of cortical representation of orbital skin and penetration 1 is 3 mm; distance between orbital skin and upper lip is about 4 cm). Therefore the CMF for this area of skin in the human may be smaller than in the macaque by a factor of 2 *(195)*.

3.5. INTRAOPERATIVE IOS IMAGING OF CORTICAL STIMULATION AT MULTIPLE WAVELENGTHS

Currently several groups are performing human IOS imaging of functional architecture and drawing conclusions about human physiology. However, little is known about the IOS response in humans at different wavelengths. We are currently investigating the IOS characteristics following a reproducible, focal cortical stimulus recorded at multiple wavelengths in the human. A two-contact ECoG strip is placed on the cortex underneath a 5 × 5-cm glass footplate. The operating room is darkened, and the cortex illuminated with a ring illuminator at 546 ± 10 nm to record the surface blood vessel pattern and then at 546 ± 10, 605 ± 10, and 700 ± 10 nm for IOS imaging. The optical reflectance signal is recorded a 10-bit camera (Imager 3001, Optical Imaging Inc., Germantown, NY) and digitized onto a PC at 33 frames per second, and integrated to variable frame rates from 10-2 frames/s. Constant current stimulation (Ojemann Cortical Stimulator, Radionics) was applied (3 s, 60 Hz, biphasic square waves of 0.5 ms duration each) at 4 mA.

We find that the optical signal recorded at 546 nm, corresponding with cerebral blood volume, is larger, both in magnitude (8%) and area, than the signal recorded at higher wavelengths (605 nm, 1.1%; 700 nm, 0.7%; ANOVA $p < 0.01$; SNK post-hoc test; Fig. 17). The signal at 546 spreads along the

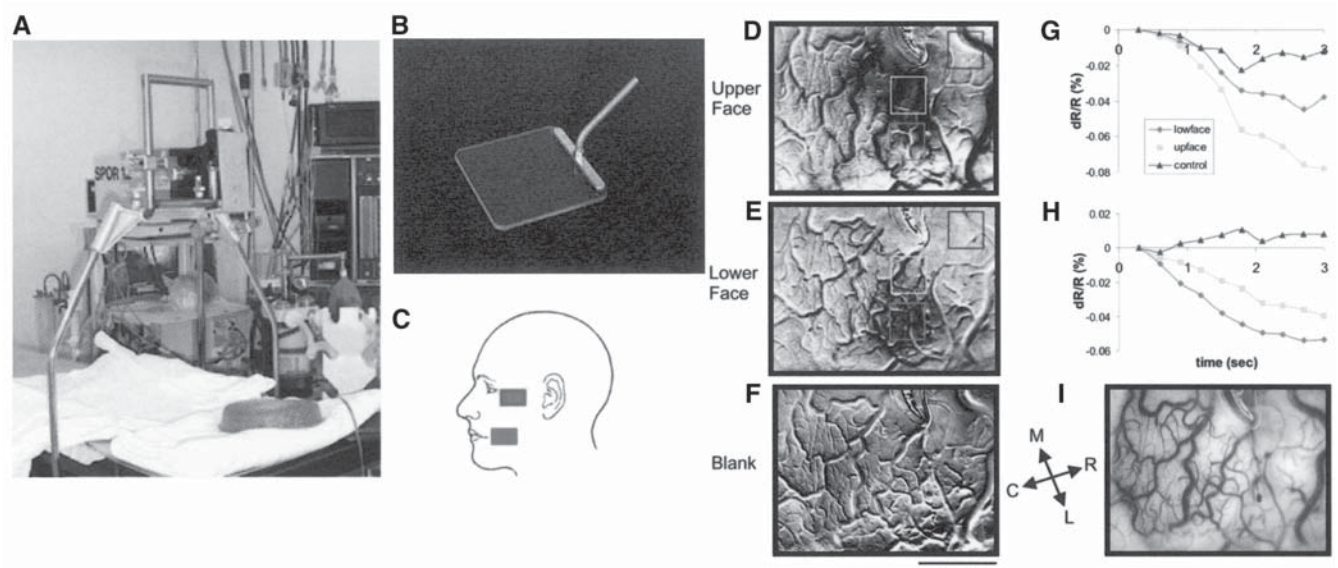

Fig. 16. **(A)** The camera is suspended above the head by attaching it to a U-bar, which is attached to the operating table on either side of the patient's chest. An X, Y, Z-manipulator holds the camera. **(B)** A glass footplate held by a retractor arm is gently placed on the cortical surface to dampen cortical pulsations. **(C)** Location of stimulating electrodes on the face. **(D)** Activation to stimulation of upper face. Sum of five trials. **(E)** Activation to stimulation of lower face. Sum of five trials. **(F)** No stimulation condition. (D) Time course of signals obtained during stimulation of upper face. Three locations were evaluated: red box is located over the lower face site, yellow box is located over the upper face site, and blue box is located over a site away from the activated sites. **(G)** Activation of upper face produces large reflectance change over the upper face location (yellow square), smaller reflectance changes over the lower face location (red box), and little change over the control location (blue triangle). **(H)** Time course of signals obtained during stimulation of lower face. Activation of lower face produces large reflectance change over lower face location, smaller reflectance change over upper face location, and little change over control location. Scale bar,5 mm. **(I)** Blood vessel map of imaged field of view. R, rostral; C, caudal; M, medial; L, lateral. *See* color version on Companion CD.

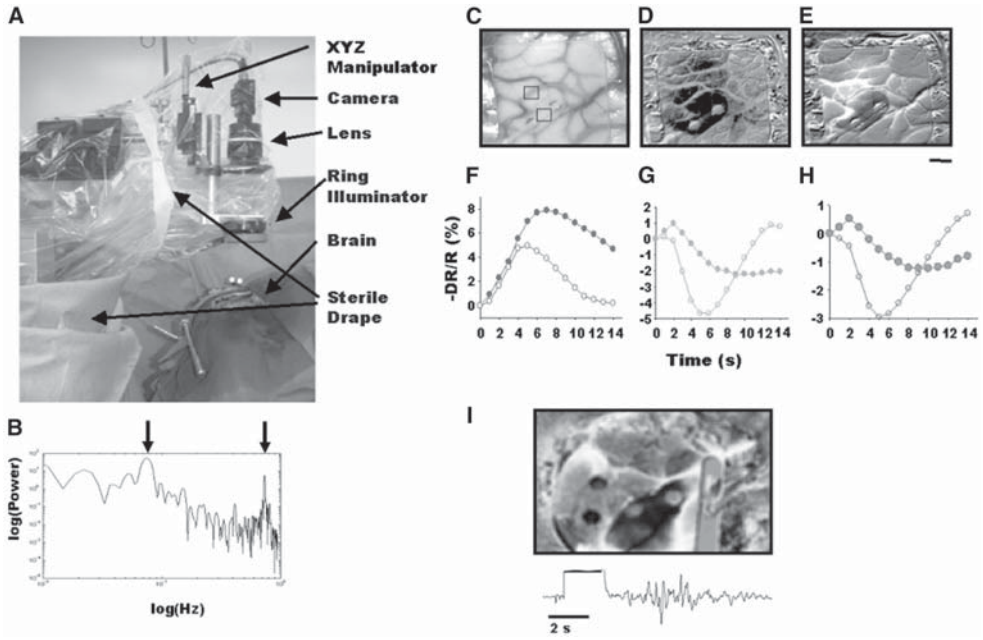

Fig. 17. (A) The camera holder is draped and the camera and ring illuminator suspended over the cortex. Using a glass footplate for cortical stabilization, we can image bipolar cortical stimulation (3 s, 60 Hz, biphasic square waves of 0.5 msec duration each and amplitude 4 mA) averaged over five trials, and **(I)** afterdischarges at 546 ± 10 nm **(D)** and 605 ± 10 nm **(E)**. **(C)** Location of the bipolar electrode on the cortical surface and the glass footplate. **(F–H)** Change in reflectance of light from two separate regions of interest. The filled circles show reflectance change in the region of interest located between the stimulating electrodes (lower box in [C]), and the open circles are from the region enclosed by the upper box in (C). Imaging was performed at 546 nm (F), 605 nm (G), and 700 nm (H). **(B)** Fourier transform of a single pixel shows that the noise associated with human imaging is mainly from vasomotor noise (left arrow) at 0.1 Hz and heart beat (right arrow) at 1 Hz. **(I)** Stimulation at a higher amplitude (10 mA) produces afterdischarges seen in ECoG recording below and a large change in reflectance in the area of the stimulating electrodes. *See* color version on Companion CD.

brain parenchyma and does not involve the blood vessels themselves. At 605 nm and 700 nm, we see an early focal decrease in reflectance in the brain parenchyma between the electrodes, consistent with the "initial dip" in oxygenation associated with metabolism that peaks at 2 s after the start of the stimulus (closed circles). A second, later and larger inverted IOS (open circles), peaking at 5 s, arises from both parenchyma and vessels, extending over approximately the same larger area as the darkening signal at 546 nm. The significance of these results will be discussed below.

3.6. INTRAOPERATIVE IOS OF EPILEPTIFORM EVENTS

Haglund et al. *(102)* first imaged afterdischarges triggered with bipolar stimulation in 1992. We have successfully repeated these experiments (Fig. 17I). However, there have been no reports of IOS imaging of spontaneous epileptiform events recorded from the human and correlated with intraoperative ECoG. We have attempted to record spontaneous IIS from human cortex and have found that the noise is a more significant factor than in studies involving sensory mapping or bipolar stimulation. We have tried to average among multiple IIS to improve our signal-to-noise ratio; however, if there is a fluctuation in the location of each IIS, the signals will cancel out. It is likely the amplitude of the IOS change associated with each IIS in chronic human epilepsy is much smaller than in the acute animal models described earlier. Other post-hoc methods to eliminate contamination from noise will have to be implemented, such as FT and PCA (discussed below).

4. CONCLUSIONS

IOS imaging is clearly a valuable technique in the study of epileptogenesis. As we have shown, the data are complementary to electrographic data and provide quantitative spatial information about blood volume, flow, and oxygenation of hemoglobin associated with the neuronal population activity underlying a variety of epileptiform events. Using several experimental models, as well as the human, we have explored the relationship between the intrinsic signal and the electrophysiology of interictal and ictal events. Although much of the

data is consistent, some is contradictory and there are many unanswered questions.

4.1. 546 NM

The signal recorded at 546 nm, thought to show changes in blood volume, is clearly the highest in amplitude. In all models, this signal peaks latest, rises more slowly, and appears to arise from the brain parenchyma and not the blood vessels. However, with 10-Hz temporal resolution, we show that as early as 100 ms after the acute disinhibition IIS, there is a focal change in reflectance at 546 nm in many of the animals we studied, a finding that is surprising because blood volume is not supposed to respond so rapidly to neuronal activity. We hypothesize that the acute disinhibited focus is a special case in which a large population of neurons is all firing simultaneously and the demand for increased blood volume is extreme. Alternatively, blood volume may in fact respond more quickly than previously thought even under physiologic circumstances, and it requires a model with an enormous focal metabolic demand with a large signal amplitude to record it.

The signal at 546 is also thought to be less focal and, hence, less sensitive to the population of active neurons. Our data are consistent with this hypothesis particularly in the human imaging. The spread of bipolar stimulation recorded at 546 nm went far beyond the bipolar stimulating electrode to the adjacent 2 or 3 gyri in the absence of afterdischarges. At such low amplitudes (4 mA), focal cortical stimulation is known to disrupt or activate only local neuronal populations, which is why it is a useful technique or brain mapping in the operating room. Hence, imaging at 546 nm does appear to overestimate the population of active neurons, unless there is a large region of subthreshold excitation which is revealed at 546 nm and not other wavelengths.

Our data in the rat, during IIS and ictal events, however, is not in agreement with the human data. Although the area of spread was larger at 546 nm in some animals, on average, there was no significant difference compared with higher wavelengths. Once again, this result may be unique to acute pharmacologically induced epileptic events in the brain, in which metabolic demands are so high, in such a large area of cortex, that the oxy-deoxy signal is as widespread as the blood volume signal.

At 546 nm, the inverted optical signal from the "surround" is less intense than at higher wavelengths in the ictal model, but not in the interictal model. In contrast, in the human, following bipolar stimulation, we were not able to record any negative signal whatsoever at 546 nm. It is not clear what the significance is of the inverted signal at 546 nm. Whether it represents shunting of blood volume to the interictal focus or an indirect marker for neuronal inhibition (or both) is unclear and will require further investigation. However, in the chronic model, the negative signal at 546 nm is clearly present, particularly during spike-and-wave activity and its disappearance during faster activity appears to correlate with horizontal spread of the seizure.

4.2. 605 AND 630 NM

IOS imaging between 600 and 650 is thought to represent changes in oxy/deoxyhemoglobin. In all experiments at these wavelengths, we observe a focal decrease in light reflectance (darkening) in the brain parenchyma that occurs within 100 ms of the event. The signal rises more rapidly than at 546 nm, peaks earlier and, in the human, and some animal experiments, is more focal. We suggest this represents the "initial dip", or decrease in oxygenation resulting from an increase in metabolism. Following this initial dip we then see an inversion in the signal, particularly in the draining veins that is less well-localized, which likely represents an increase in blood flow and a rise in oxygenated hemoglobin as found in the blood oxygen level dependent signal. However, there is another inverted signal that occurs early in the brain parenchyma in the surrounding cortex. In our fast imaging experiments, this signal begins within 100 ms. We propose that this signal may correspond to surround inhibition; the relative timings of the signals may be critical in distinguishing these two distinct inverted signals.

4.3. 700 NM

Our results at 700 nm are quite similar to our results at 605 and 630 nm, although the signal is smaller in amplitude and more focal. Reflected light at 700 nm is believed to represent cell swelling; however, we do not employ an absorption filter and there may be significant contamination from the oxy/deoxyhemoglobin signal. We anticipated that the signal at this wavelength would be more rapid than at 605 or 630 nm, but this was not observed. The focality of the change in reflection may imply that it is an even better signal for localizing the population of epileptic neurons. Correlation with multifocal single-unit and f.p. recordings may answer this question.

4.4. INVERTED IOS

Whether the inverted IOS recorded from the surrounding brain parenchyma as early as 100 ms after the IIS represents shunting of blood volume, oxygenation, or, indirectly, neuronal inhibition, is unclear. Single unit recordings from the inverted optical signal region adjacent to a BMI-induced interictal focus in the ferret found decreased neuronal activity *(100)*. Das and Gilbert *(20)* observed an increase in reflectance in the cat primary visual cortex that they hypothesize may be an "inhibitory moat surrounding the excitatory center." Similarly, single-unit recordings from a ring of inverted optical signal in mouse visual cortex, in response to retinotopic photic stimulation, also revealed neuronal inhibition *(19)*.

However, Haglund et al. *(102)* raised the possibility that the increase in light reflectance may result from a decrease in blood flow, resulting from a shunting of blood toward the focus, rather than from a decrease in electrophysiologic activity. We found, in our interictal model, an early, wavelength-independent, inverted signal, and in our ictal and human studies, a late inverted wavelength-dependent signal. We hypothesize that the early wavelength-independent inverted signal is more likely to correlate with neuronal inhibition than the later signal. Our future experiments will explore this question using muticontact electrodes, voltage-sensitive dyes and other methods for measuring blood volume (Texas Red Dextran) in our epilepsy models.

4.5. ANALYSIS TECHNIQUES

The classic technique for IOS image analysis has been to divide images acquired during an activated state by images acquired during an inactive state. Image acquisition is triggered by stimulus onset. Fluctuations in the signal that are not related to the stimulus are removed by trial repetition and signal averaging. Recently, there has been rising interest in applying other methods of analysis to the intrinsic signal. There are several

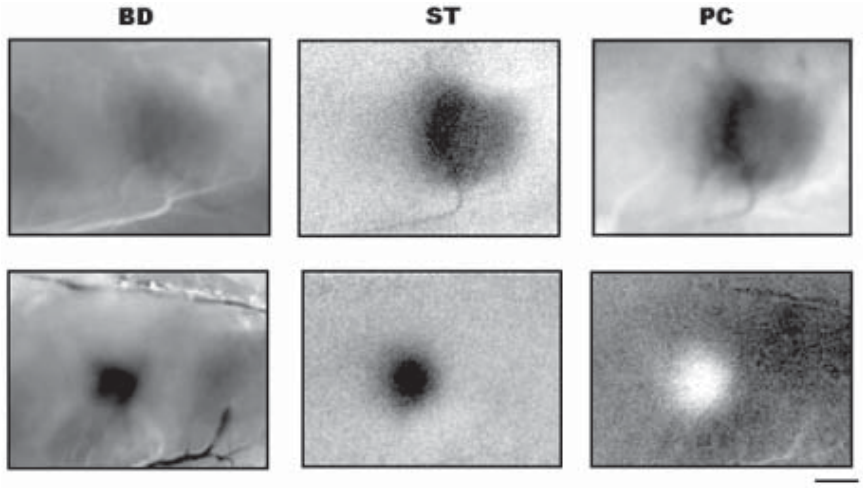

Fig. 18. Image analysis is compared using blank divided (BD), spike-triggered (ST), and PCA (PC). All three maps are comparable. The BD and ST maps are calculated with image division, whereas the PCA maps are calculated from the raw signal. There is more vascular noise in the BD maps because several minutes separated the denominator frame from the numerator frame. Scale bar, 1 mm.

limitations to requiring the use of a "blank" state for image division. The cortex is always active, so a true "blank" is impossible to achieve. Any signal within the blank will introduce signal into the final image (e.g., Fig. 10). The experiments take twice as long since an equal number of blank images must be acquired. Lengthy experimentation is also a necessity if trial averaging is used to reduce noise. For epilepsy imaging, these two issues are particularly bothersome. In chronic epilepsy, the focus is constantly spiking and so there is no "blank" state when nothing is happening. Likewise, as discussed earlier, each epileptiform event is different and the dynamic fluctuations in the epileptic pool of neurons make averaging between events counterproductive. Two interesting methods for addressing these problems are FT and PCA *(33,34)*. We have begun exploring both methods as a means of eliminating noise with a known periodicity. However, to extract epileptic data, one must know the periodicity of the signal of interest. For acute interictal spikes that occur with a regular periodicity, the epileptic intrinsic signal can be easily extracted (Fig. 18). However, in chronic epilepsy, the periodicity of the epileptiform events is irregular and signal extraction is much more difficult. Nevertheless, as technology and computational sophistication improve, many of our current obstacles will be overcome. The ultimate role for IOS imaging in the treatment of epilepsy has yet to be determined, but the outlook is promising.

ACKNOWLEDGMENTS

This work was supported by NINDS (K08, R21), as well as grants from the Alexander von Humboldt Fellowship, Van Wagenen Fellowship of the American Association for Neurological Surgeons (AANS), Research Clinical Training Grant from the Epilepsy Foundation of America, DANA Foundation, CURE Foundation, and Junior Clinical Investigator Award from the AANS. We thank our collaborators, including Tobias Bonhoeffer, Mark Hubener, Frank Sengpiel, Sven Shuett, Anna Roe, Dennis Spencer, Robert Friedman, Li-Min Chen and Amiram Grinvald, as well as Koon-Ho Danny Wong for technical assistance.

REFERENCES

1. Hill DK, Keynes RD. Opacity changes in stimulated nerve. J Physiol 1949;108:278–281.
2. Chance BC, P., Jobsis F, Schoener B. Intracellular oxidation-reduction states in vivo. Science 1962;137:499–508.
3. Jobsis FF. Noninvasive, infrared monitoring of cerebral and myocardial oxygen sufficiency and circulatory parameters. Science 1977;198:1264–1266.
4. Cohen LB, Keynes RD. Changes in light scattering associated with the action potential in crab nerves. J Physiol 1971;212:259–275.
5. Cohen L. Optical approaches to neuronal function. In: Hoffman JF, De Weer P, eds. Annual Review of Physiology. Palo Alto, CA: Annual Review Inc.; 1989:487–582.
6. Grinvald A, Lieke EE, Frostig RD, Gilbert CD, Wiesel TN. Functional architecture of cortex revealed by optical imaging of intrinsic signals. Nature 1986;324:361–364.
7. Bonhoeffer T, Grinvald A. Iso-orientation domains in cat visual cortex are arranged in pinwheel-like patterns. Nature 1991;353:429–431.
8. Bonhoeffer T, Grinvald A. The layout of iso-orientation domains in area 18 of cat visual cortex: optical imaging reveals a pinwheel-like organization. J Neurosci 1993;13:4157–4180.
9. Rubin BD, Katz LC. Optical imaging of odorant representations in the mammalian olfactory bulb. Neuron 1999;23:499–511.

10. Mrsic-Flogel T, Hübener M, Bonhoeffer T. Brain mapping: new wave optical imaging. Curr Biol 2003;13.:R778–R780.
11. Bonhoeffer T, Grinvald A. Optical imaging based on intrinsic signals. The methodology. In: Toga AW, Mazziota JC, eds. Brain Mapping The Methods. San Diego: Academic Press; 1996:55–99.
12. Holthoff K, Witte OW. Intrinsic optical signals in rat neocortical slices measured with near-infrared dark-field microscopy reveal changes in extracellular space. J Neurosci 1996;16:2740–2749.
13. Frostig RD, Lieke EE, Ts'o DY, Grinvald A. Cortical functional architecture and local coupling between neuronal activity and the microcirculation revealed by in vivo high-resolution optical imaging of intrinsic signals. Proc Natl Acad Sci 1990;87:6082–6086.
14. Malonek D, Grinvald A. Interactions between electrical activity and cortical microcirculation revealed by imaging spectroscopy: implications for functional brain mapping. Science 1996;272:551–554.
15. Vanzetta I, Grinvald A. Increased cortical oxidative metabolism due to sensory stimulation: implications for functional brain imaging. Science 1999;286:1555–1558.
16. Pouratian N, Sicotte N, Rex D, et al. Spatial/temporal correlation of BOLD and optical intrinsic signals in human. Magn Res Med 2003;47:766–776.
17. Fox PT, Raichle ME. Focal physiological uncoupling of cerebral blood flow and oxidative metabolism during somatosensory stimulation in human subjects. Proc Natl Acad Sci USA 1986;83:1140–1144.
18. Kwong KK, Belliveau JW, Chesler DA, et al. Dynamic magnetic resonance imaging of human brain activity during primary sensory stimulation. Proc Natl Acad Sci USA 1992;89:5675–5679.
19. Schuett S, Bonhoeffer T, Hubener M. Mapping retinotopic structure in mouse visual cortex with optical imaging. J Neurosci 2002;22: 6549–6559.
20. Das A, Gilbert CD. Long-range horizontal connections and their role in cortical reorganization revealed by optical recording of cat primary visual cortex. Nature 1995;375:780–784.
21. Toth LJ, Rao SC, Kim DS, Sur M. Subthreshold facilitation and suppression in primary visual cortex revealed by intrinsic signal imaging. Proc Natl Acad Sci USA 1996;93:9869–9874.
22. Hübener M, Shoham D, Grinvald A, Bonhoeffer T. Spatial relationships among three columnar systems in cat area 17. J Neurosci 1997; 17:9270–9284.
23. Sengpiel F, Stawinski P, Bonhoeffer T. Influence of experience on orientation maps in cat visual cortex. Nature Neurosci 1999;2:727–732.
24. Issa NP, Trachtenberg JT, Chapman B, Zahs KR, Stryker MP. The critical period for ocular dominance plasticity in the ferret's visual cortex. J Neurosci 1999;19:6965–6978.
25. Chapman B, Bonhoeffer T. Overrepresentation of horizontal and vertical orientation preferences in developing ferret area 17. Proc Natl Acad Sci USA 1998;95:2609–2614.
26. White LE, Bosking WH, Williams SM, Fitzpatrick D. Maps of central visual space in Ferret V1 and V2 lack matching inputs from the two eyes. J Neurosci 1999;19:7089–7099.
27. Schwartz TH. Optical imaging of epileptiform events in visual cortex in response to patterned photic stimulation. Cereb Cortex 2003; 13:1287–1298.
28. Fitzpatrick D. The functional organization of local circuits in visual cortex: insights from the study of tree shrew cortex. Cereb Cortex 1996;6:329–341.
29. Weliky M, Bosking WH, Fitzpatrick D. A systematic map of direction preference in primary visual cortex. Nature 1996;379:725–728.
30. Grinvald A, Frostig RD, Siege RM, Bartfeld E. High-resolution optical imaging of functional brain architecture in the awake monkey. Proc Natl Acad Sci U S A 1991;88:11559–11563.
31. Roe AW, Ts'o DY. Specificity of color connectivity between primate V1 and V2. J Neurophysiol 1999;82:2719–2730.
32. Bonhoeffer T, Kim D-S, Maloniek, Shoham D, Grinvald A. Optical imaging of the layout of functional domains in area 17 and across the area 17/18 border in cat visual cortex. Eur J Neurosci 1995;7:1973–1988.
33. Kalatsky VA, Stryker MP. New paradigm for optical imaging: temporally encoded maps of intrinsic signal. Neuron 2003;38:529–545.
34. Sornborger A, Sailstad C, Kaplan E, Sirovich L. Spatiotemporal analysis of optical imaging data. NeuroImage 2003;18:610–621.
35. Brett-Green BA, Chen-Bee CH, Frostig RD. Comparing the functional representations of central and border whiskers in rat primary somatosensory cortex. J Neurosci 2001;21:9944–9954.
36. Takashima I, Kajiwara R, Iijima T. Voltage-sensitive dye versus intrinsic signal optical imaging: comparison of optically determined functional maps from rat barrel cortex. Neuroreport 2001;12:2889–2894.
37. Sheth SA, Nemoto M, Guiuo M, Walker M, Pouratian N, Toga AW. Evaluation of coupling between optical intrinsic signals and neuronal activity in rat somatosensory cortex. NeuroImage 2003;19: 884–894.
38. Shoham D, Grinvald A. The cortical representation of the hand in macaque and human area S-1: high resolution optical imaging. J Neurosci 2001;21:6820–6835.
39. Chen LM, Friedman RM, Ramsden BM, LaMotte RH, Roe AW. Fine-scale organization of S1 (Area 3b) in the squirrel monkey revealed with intrinsic optical imaging. J Neurophysiol 2001;86:3011–3029.
40. Chen LM, Friedman RM, Ramsden BM, Roe AW. Organization of the somatosensory cortex revealed with intrinsic optical imaging in the squirrel monkey. Soc Neurosci Abstr 1999;25:1167.
41. Arieli A, Grinvald A, Slovin H. Dural substitute for long-term imaging of cortical activity in behaving monkeys and its clinical implications. J Neurosci Methods 2002;114:119–133.
42. Leão AAP. Pial circulation and spreading depression of activity in the cerbral cortex. J Neurophysiol 1944;7:391–396.
43. Leão AAP. Spreading depression of activity in the cerebral cortex. J Neurophysiol 1944;7:259–390.
44. Martins-Ferreira H, Nedergaard M, Nicholson C. Perspectives on spreading depression. Brain Res Rev 2000;32:215–234.
45. Richter F, Lemenkühler A. Spreading depression can be restricted to distinct depths of the rat cerebral cortex. Neurosci Lett 1993;152: 65–68.
46. Ba AM, Guiou G, Pouratian N, et al. Multiwavelength optical intrinsic signal imaging of cortical spreading depression. J Neurophysiol 2002;10:2726–2735.
47. Hossmann KA. Glutamate-mediated injury in focal cerebral ischemia: the excitotoxin hypothesis revised. Brain Pathol 1994; 4:23–36.
48. Koroleva VI, Bures J. Blockade of cortical spreading depression in electrically and chemically stimulated areas of cerebral cortex in rats. EEG Clin Neurophysiol 1980;48:1–15.
49. Aitken PG, Tombaugh GC, Turner DA, Somjen GG. Similar propagation of SD and hypoxic SD-like depolarization in rat hippocampus recorded optically and electrically. J Neurophysiol 1998;80:1514–1521.
50. Peixonto NL, Fernandes de Lima VM, Hanke W. Correlation of the electrical and intrinsic optical signals in the chicken spreading depression phenomenon. Neurosci Lett 2001;299:89–92.
51. Müller M, Somjen GG. Intrinsic optical signals in rat hippocampal slices during hypoxia induced spreading depression-like depolarization. J Neurophysiol 1999;82:1818–1831.
52. Bahar S, Fayuk D, Somjen GG, Aitken PG, Turner DA. Mitochondrial depolarization and intrinsic optical signal Imaged during hypoxia and spreading depression in rat hippocampal slices. J Neurophysiol 2000;84:311–324.
53. O'Farrell AM, Rex DE, Jmutialu A, et al. Characterization of optical intrinsic signals and blood volume during cortical spreading depression. Neuroreport 2000;11:2121–2125.
54. Hauser WA, Hesdorfer DC. Epilepsy: frequency, causes and consequences. New York: Demos; 1990.
55. Fisher RS, Weber WR, Lesser RP, Aroyo S, Uematsu S. High-frequency EEG activity at the start of seizures. J Clin Neurophsyiol 1992;9:441–448.
56. Bragin A, Mody I, Wilson CL, Engel JJ. Local generation of fast ripples in epileptic brain. J Neurosci 2002;22:2012–2021.
57. Staba RJ, Wilson C, Bragin A, Fried I, Engel JJ. Quantitative analysis of high-frequency oscillations(80–500 Hz) recorded in human epileptic hippocampus and entorhinal cortex. J Neurophysiol 2002;88:1743–1752.

58. Ylinen A, Bragin A, Nádasdy Z, et al. Sharp wave associated high frequency oscillation (200 Hz) in the intact hippocampus: network and intracellular mechanisms. J Neurosci 1995;14:30–46.
59. Grenier F, Timofeev I, Steriade M. Neocortical very fast oscillations (ripples, 80–200 Hz) during seizures: intracellular correlates. J Neurophysiol 2003;89:841–852.
60. Traub RD, Whittington MA, Buhl EH, et al. A possible role of gap junctions in generating very fast EEG oscillations preceding the onset of, and perhaps initiating, seizures. Epilepsia 2001;42:153–170.
61. Schwartzkroin PA. Epilepsy. Models, Mechanisms and Concepts. Cambridge: Cambridge University Press; 1993.
62. Matsumoto H, Ajmone-Marsan C. Cortical cellular phenomena in experimental epilepsy: interictal manifestations. Exp Neurol 1964;9: 286–304.
63. Matsumoto H, Ajmone-Marsan C. Cortical cellular phenomena in experimental epilepsy: ictal manifestations. Exp Neurol 1964;9:305–326.
64. Prince DA. The depolarizing shift in "epileptic" neurons. Exp Neurol 1968;21:467–485.
65. Chagnac-Amitai Y, Connors BW. Synchronized excitation and inhibition driven by intrinsically bursting neurons in neocortex. J Neurophysiol 1989;62:1149–1162.
66. Chagnac-Amitai Y, Connors BW. Horizontal spread of synchronized activity in neocortex and its control by GABA mediated inhibition. J Neurophysiol 1989;61:747–758.
67. Chervin RD, Pierce PA, Connors BW. Periodicity and directionality in the propagation of epileptiform discharges across neocortex. J Neurophysiol 1988;60:1695–1713.
68. Connors BW. Initiation of synchronized bursting in neocortex. Nature 1984;310:685–687.
69. Telfian AE, Connors BW. Layer-specific pathways for the horizontal propagation of epileptiform discharges in neocortex. Epilepsia 1998;39:700–708.
70. Gutnick MJ, Connors BW, Prince DA. Mechanisms of neocortical epileptogenesis in vitro. J Neurophysiol 1982;48:1321–1335.
71. de Lanerolle NC, Kim JH, Robbins RJ, Spencer DD. Hippocampal interneuron loss and plasticiy in human temporal lobe epilepsy. Brain Res 1989;495:387–395.
72. Prince DA, Jacobs KM, Salin PA, Hoffman S, Parada I. Chronic focal neocortical epileptogenesis: does disinhibition play a role? Can J Physiol Pharmacol 1997;75:500–507.
73. Schwartzkroin PA, Haglund MM. Spontaneous rhythmic activity in epileptic human and normal monkey temporal lobe. J Neurophysiol 1986;27:523–533.
74. Davenport CJ, Brown WJ, Babb TL. Sprouting of GABAergic and mossy fiber axons in dentate gyrus following intrahippocampal kainate injections in the rat. Exp Neurol 1990;109:180–190.
75. Nusser Z, Hajos N, Somogyi P, Mody I. Increased numbers of synaptic GABA(A) receptors underlies poteniation at hippocampal inhibitory synapses. Nature 1998;395:172–177.
76. Esclapez M, Hirsch JC, Khazipov R, Ben Ari Y, Bernard C. Operative GABAergic inhibition in hippocampal CA1 pyramidal neurons in experimental epilepsy. Proc Natl Acad Sci USA 1997;94:12151–12156.
77. Isokawa-Akeson M, Wilson CL, Babb TL. Inhibition in synchronously firing human hippocampal neurons. Epilepsy Res 1989;3:236–247.
78. Colder BW, Frysinger RC, Wilson CL, Harper M, Engel JJ. Decreased neuronal burst discharge near site of seizure onset in epileptic human temporal lobes. Epilepsia 1996;37:113–121.
79. Kisvárday ZF. GABAergic networks of basket cells in the visual cortex, In: Mize RR, Marc R, Sillito AM, eds. Progress in Brain Research, Vol 90, Mechanisms of GABA in the Visual System. Amsterdam: Elsevier; 1992:385–405.
80. Andersen P, Eccles JC, Løyning Y. Pathway of postsynaptic inhibition in the hippocampus. J Neurophysiol 1964;27:608–619.
81. Dichter M, Spencer WA. Penicillin-induced interictal discharges from cat hippocampus. I. Characteristics and topographical features. J Neurophysiol 1969;32:649–662.
82. Prince DA, Wilder J. Control mechanisms in cortical epileptogenic foci. "Surround" inhibition. Arch Neurol 1967;16:194–202.
83. Goldensohn ES, Salazar AM. Temporal and spatial distribution of intracellular potentials during generation and spread of epileptogenic discharges. Adv Neurol 1986;44:559–582.
84. Tucker TR, Katz LC. Recruitment of local inhibitory networks by horizontal connections in layer 2/3 of ferret visual cortex. J Neurophysiol 2003;89:501–512.
85. Tucker TR, Katz LC. Spatiotemporal patterns of excitation and inhibition evoked by the horizontal network in layer 2/3 of ferret visual cortex. J Neurophysiol 2003;89:488–500.
86. Duncan JS. Imaging and epilepsy. Brain 1997;120:339–377.
87. Pedley TA. Interictal epileptiform discharges: discriminating characteristics and clinical correlations. AM J EEG Technol 1980;20:101–119.
88. Dichter MA, Ayala GF. Cellular mechanisms of epilepsy: a status report. Science 1987;237:157–164.
89. McNamara JO. Cellular and molecular basis of epilepsy. J Neurosci 1994;14:3413–3425.
90. Wyler AR, Burchiel KJ, Ward AAJ. Chronic epileptic foci in monkeys: correlation between seizure frequency and proportion of pacemaker neurons. Epilepsia 1978;19:475–483.
91. Prince DA, Futamachi KJ. Intracellular recordings from chronic epileptogenic foci in the monkey. Electroencephalogr Clin Neurophysiol 1970;29:496–510.
92. Cohen I, Navaro V, Clemenceau S, Baulac M, Miles R. On the origin of interictal activity in human temporal lobe epilepsy in vitro. Science 2002;298:1418–1421.
93. Penfield W. The evidence for cerebral vascular mechanism in epilepsy. Ann Intern Med 1933;7:303–310.
94. Hochman DW, Baraban SC, Owens JWM, Schwartzkroin PA. Dissociation of synchronization and excitability in furosemide blockade of epileptiform activity. Science 1995;270:99–102.
95. Buchheim K, Schuchmann S, Siegmund H, Weissinger F, Heinemann U, Meierkord H. Comparison of intrinsic optical signals associated with low Mg2+-and 4-aminopyridine-induced seizure-like events reveals characteristic features in the adult rat limbic system. Epilepsia 2000;41:635–641.
96. Weissinger F, Buchheim K, Siegmund H, Heinemann U, Meierkord H. Optical imaging reveals characteristic seizure onsets, spread patterns, and propagation velocities in hippocampal-entorhinal cortex slices of juvenile rats. Neurobiol Dis 2000;7:286–298.
97. D'Arcangelo G, Tancredi V, Avoli M. Intrinsic optical signals and electrographic seizures in the rat limbic system. Neurobiol Dis 2001; 8:993–1005.
98. Federico P, Borg SG, Salkauskus AG, MacVicar BA. Mapping patterns of neuronal activity and seizure propagation in the isolated whole brain of the guinea-pig. Neuroscience 1994;58:461–480.
99. Chen JWY, O'Farrell AM, Toga AW. Optical intrinsic signal imaging in a rodent seizure model. Neurology 2000;55:312–315.
100. Schwartz TH, Bonhoeffer T. In vivo optical mapping of epileptic foci and surround inhibition in ferret cerebral cortex. Nat. Med 2001; 7:1063–1067.
101. Haglund MM, Blasdel GG. Optical imaging of acute epileptic foci in monkey visual cortex. Epilepsia 1993;34:21.
102. Haglund MM, Ojemann GA, Hochman DW. Optical imaging of epileptiform and functional activity in human cerebral cortex. Nature 1992;358:668–671.
103. Engel JJ, Shewmon DA. Who should be considered a surgical candidate?, In: Engel JJ, ed. Surgical Treatment of the Epilepsies. New York: Raven Press; 1993:23–34.
104. Buzsáki G, Traub RD. Physiological basis of EEG activity, In: Engel TA, Pedley TA, ed. Epilepsy: A Comprehensive Textbook. Philadelphia: Lippincott-Raven Publishers; 1997:819–830.
105. Gloor P. Neuronal generators and the problem of localization in electroencephalography: application of volume conduction theory to electroencephalography. J Clin Neurophysiol 1985;2:327–354.
106. Alarcon G, Guy CN, Binnie CD, Walker SR, Owes R, Polkey CE. Intracerebral propagation of interictal spikes in partial epilepsy: implications for source localization. J Neurol Neurosurg Psychiatry 1994;57:435–449.
107. Uematsu D, Araki N, Greenberg JH, Reivich M. Alterations in cytosolic free calcium in the cat cortex during bicuculline-induced epilepsy. Brain Res Bull 1990;24:285–288.

108. Purpura DP, Pernry JK, Tower D, Woodbury DM, Walter R. Experimental Models of Epilepsy - A Manual for the Laboratory Worker. New York: Raven Press; 1972.
109. Fisher RS. Animal models of the epilepsies. Brain Res Rev 1989; 14:245–278.
110. Prince DA. Topical convulsant drugs and metabolic antagonists, In: Purpura DP, Penry JK, Tower DB, Woodbury DM, Walter RD, eds. Experimental Models of Epilepsy—A Manual for the Laboratory Worker. New York: Raven Press; 1972:52–83.
111. Szente M, Pongracz F. Aminopyridine-induced seizure activity. Electroencephalogr Clin Neurophysiol 1979;46:605–608.
112. Szente BM, Baranyi A. Mechanism of aminopyridine-induced ictal seizure activity in the cat neocortex. Brain Res 1987;41:386–373.
113. Ajmone Marsan C. Focal electrical stimulation, In: Purpura DP, Penry JK, Tower DB, Woodbury DM, Walter RD, ed. Experimental Models of Epilepsy—A Manual for the Laboratory Worker. New York: Raven Press; 1972:148–169.
114. Bashir ZI, Holmes O. Phases in the development of a penicillin epileptiform focus in rat neocortex. Exp Brain Res 1993;96:319–327.
115. Campbell A, Homes O. Bicuculline epileptogenesis in the rat. Brain Res 1984;323:239–246.
116. Petsche H, Prohaska O, Rappelsburger P, Vollmer R, Kaiser A. Cortical seizure patterns in a multidimensional view: the information content of equipotential maps. Epilepsia 1974;15:439–463.
117. Goldensohn ES, Zablow L, Salazar A. The penicillin focus. I. Distribution of potential at the cortical surface. Electroencephalogr Clin Neurophysiol 1977;42:480–492.
118. Wyler AR, Ward AAJ. Epileptic neurons, In: Lockard JSS, Ward AAJ, eds. Epilepsy: A Window to Brain Mechanisms. New York: Raven; 1980: 51–68.
119. Wyler AR, Ojemann GA, Ward AA, Jr. Neurons in human epileptic cortex: correlation between unit and EEG activity. Ann Neurol 1982;11:301–308.
120. Ishijima B, Hori T, Yoshimasu N, Fukushima T, Hirakawa K, Seikino H. Neuronal activities in human epileptic foci and surrounding areas. EEG Clin Neurophysiol 1975;39:643–650.
121. Mattia D, Haw GG, Avoli M. Epileptiform activity induced by 4-aminopyridine in guinea-pig and rat neocortices. Neurosci Lett 1993;154:157–160.
122. Stansfeld CE, Marsh SJ, Halliwell JV, Brown D. 4-Aminopyridine and dendrotoxin induce repetitive firing in rat visceral sensory neurons by slowly inactivating outward current. Neurosci Lett 1986;64: 299–304.
123. Barkai E, Friedman A, Grossman Y, Gutnick MJ. Laminar pattern of synaptic inhibition during convulsive activity induced by 4-aminopyridine in neocortical slices. J Neurophysiol 1995;73:1462–1467.
124. Benardo LS. Recruitment of GABAergic inhibition and synchronization of inhibitory interneurons in rat neocortex. J Neurophysiol 1997;77:3134–3144.
125. Rogawski MA, Barker JA. Effects of 4-aminopyridine on calcium action potentials and calcium current under voltage clamp in spinal neurons. Brain Res 1983;280:180–185.
126. Szente BM, Baranyi A. Properties of depolarizing plateau potentials in aminopyridine-induced ictal seizure foci of cat motor cortex. Brain Res 1989;495:261–270.
127. Yang XF, Rothman SM. Focal cooling rapidly terminates experimental neocortical seizures. Ann Neurol 2001;49:721–726.
128. Yang XF, Chang JH, Rothman SM. Intracerebral temperature alterations associated with focal seizures. Epilepsy Res 2002;52:97–105.
129. Wong BY, Prince DA. The lateral spread of ictal discharges in neocortical brain slices. Epilepsy Res 1990;7:29–39.
130. Ratzlaff EH, Grinvald A. A tandem-lens epifluorescence microscope: hundred-fold brightness advantage for wide field imaging. J Neurosci Methods 1991;36:127–137.
131. Chen-Bee CH, Kwon MC, Masino SA, Frostig RD. Areal extent quantification of functional representations using intrinsic signal optical imaging. J Neurosci Meth 1996;68:27–37.
132. Masino SA, Kwon MC, Dory Y, Frostig R. Characterization of functional organization within rat barrel cortex using intrinsic signal optical imaging through a thinned skull. Proc Natl Acad Sci USA 1993;90:9998–10002.
133. Szente MB, Boda B. Cellular mechanisms of neocortical secondary epileptogenesis. Brain Res 1994;648:203–214.
134. Schwartzkroin PA, Futamachi KJ, Noebels JL, Prince DA. Transcallosal effects of a cortical epileptiform focus. Brain Res 1975;99:59–68.
135. Engel JJ. Surgery for seizures. N Engl J Med 1996;334:647–652.
136. Babb TL, Crandall PH. Epileptogenesis of human limbic neurons in psychomotor epileptics. EEG Clin Neurophysiol 1976;40:225–243.
137. Engel JJ. Functional explorations of the human epileptic brain and their therapeutic implications. EEG Clin Neurophysiol 1990;76:296–316.
138. Engel JJ. Intracerebral recordings: organization of the human epileptogenic region. J Clin Neurophysiol 1993;10:90–98.
139. Kutsy RL, Farrell DF, Ojemann GA. Ictal patterns of neocortical seizures monitored with intracranial electrodes: correlation with surgical outcome. Epilepsia 1999;30:257–266.
140. Spencer SS, Guimaraes P, Kim J, Spencer DD. Morphological patterns of seizures recorded intracranially. Epilepsia 1992;33:537–545.
141. Williamson A, Spencer SS, Spencer DD. Depth electrode studies and intracellular dentate granule cell recordings in temporal lobe epilepsy. Ann Neurol 1995;38:778–787.
142. Spencer SS, Spencer DD. Implications of seizure termination location in temporal lobe epilepsy. Epilepsia 1996;37:455–458.
143. Netoff TI, Schiff SS. Decreased neuronal synchronization during experimental seizures. J Neurosci 2002;22:7297–7307.
144. Ayala GF, Matsumoto H, Gumnit RJ. Excitability changes and inhibitory mechanisms in neocortical neurons during seizures. J Neurophysiol 1970;33:73–85.
145. Haycock JW, Levy WB, Cotman CW. Stimulation-dependent depression of neurotransmitter release in the brain: [Ca] dependence. Brain Res 1987;155:192–195.
146. Bragin A, Penttonen M, Buzsáki G. Termination of epileptic afterdischarge in the hippocampus. J Neurosci 1997;17:2567–2579.
147. Binnie CD, Wilkins AJ. Visually induced seizures not caused by flicker (intermittent right stimulation), In: Zifkin BG, Andermann F, Beaumanoir A, Rowan AJ, ed. Advances in Neurology. Philadelphia: Lippincott-Raven; 1998:123–138.
148. Dorothée GA, Trenité K-N. Reflex seizures induced by intermittent light stimulation, In: Zifkin BG, Andermann F, Beaumanoir A, Rowan AJ, eds. Advances in Neurology. Philadelphia: Lippincott-Raven; 1998:99–121.
149. Ribak CE, Reiffenstein RJ. Selective inhibitory synapse loss in chronic cortical slabs: a morphological basis for epileptic susceptibility. Can J Physiol Pharmacol 1982;60:864–870.
150. Prince DA, Tseng G-F. Epileptogenesis in chronically injured cortex: in vitro studies. J Neurophysiol 1993;69:1276–1291.
151. Salin P, Tseng G-F, Hoffman S, Parada I, Prince DA. Axonal sprouting in layer V pyramidal neurons of chronically injured cerebral cortex. J Neurosci 1995;15:8234–8245.
152. Lewis DV, Mutsuga N, Schuette WH. Potassium clearance and reactive gliosis in the alumna cream model. Epilepsia 1977;18:499–506.
153. Haglund MM, Berger MS, Kunkel DD, Franck JE, Ghatan S, Ojemann GA. Changes in o-aminobutyric acid and somatostatin in epileptic cortex associated with low-grade gliomas. J Neurosurg 1992;77:209–216.
154. Ward AA. Topical convulsant metals, In: Purpura DP, Penry JK, Woodbury DM, Tower DB, Walter RD, eds. Experimental Models of Epilepsy—A Manual for the Laboratory Worker. New York: Raven; 1972:13–35.
155. Prince DA, Futamachi KJ. Intracellular recordings in chronic focal epilepsy. Brain Res 1968;11:681–684.
156. Atkinson JR, Ward AAJ. Intracellular studies of cortical neurons in chronic epileptogenic foci in the monkey. Exp Neurol 1964;10:285–295.
157. Ward AAJ. The epileptic neurone. Epilepsia 1961;2:70–80.
158. Willmore LJ, Sypert GW, Munson JB, Hurd RW. Chronic focal epileptiform discharges induced by injection of iron into rat and cat cortex. Science 1978;200:1501–1503.
159. Willmore LJ, Sypert GW, Munson JB. Recurrent seizures induced by cortical iron injection: a model of posttraumatic epilepsy. Ann Neurol 1978;4:329–336.

160. Moriwaki A, Hattori Y, Nishida N, Hori Y. Electrographic characterization of chronic iron-induced epilepsy in rats. Neurosci Lett 1990;110:72–76.
161. Moriwaki A, Hattori Y, Hayashi Y, Hori Y. Development of epileptic activity induced by iron injection into rat cerebral lcortex: electrographic and behavioral characteristics. EEG Clin Neurophysiol 1992;83:281–288.
162. Willmore LJ, Rubin JJ. Antiperoxidant pretreatment and iron-induced epileptiform discharges in the rat: EEG and histopathologic studies. Neurology 1981;31:63–69.
163. Engstrom R, Hillered L, Flink R, Kihlstrom L, Lindquist C, Nie J-X, Olsson Y, Silander HC. Extracellular amino acid levels measured with intracerebral microdialysis in the model of posttraumatic epilepsy induced by intracortical iron injection. Epilepsy Research 2001;43:135–144.
164. Reid SA, Sypert GW, Boggs WM, Williams LJ. Histopathology of the ferric-induced chronic epileptic focus in the cat: a golgi study. Exp Neurol 1979;66:205–219.
165. Westrum LE, White LE, Ward AAJ. Morphology of the experimental epileptic focus. J Neurosurg 1964;21:1033–1046.
166. Schiebel ME, Crandall PH, Schiebel AB. The hippocampal-dentate complex in temporal lobe epilepsy-a golgi study. Epilepsia 1974; 15:55–80.
167. Brooks VB, Asunama H. Action of tetanus toxin in the cerebral cortex. Science 1962;137:674–676.
168. Carrea R, Lanari A. Chronic effects of tetanus toxin applied locally in the cerebral cortex of the dog. Science 1962;137:342–343.
169. Mellanby J, George G, RObinson A, Thompson PA. Epileptiform syndrome in rats produced by injecting tetanus toxin into the hippocampus. J Neurol Neurosurg Psychiatry 1977;40:404–414.
170. Brener K, Amitai Y, Jeffreys JGR, Gutnick MJ. Chronic epileptic foci in neocotex: In vivo and in vitro efects of tetanus toxin. Eur J Neurosci 1990;3:47–54.
171. Finnerty GT, Jeffreys JGR. Investigations of the neuronal aggregate generating seizures in the rat tetanus toxin model of epilepsy. J Neurophysiol 2002;88:2919–2927.
172. Louis ED, Williamson PD, Darcey TM. Chronic focal epilepsy induced by microinjection of tetanus toxin ino the cat motor cortex. EEG Clin Neurophysiol 1990;75:548–557.
173. Hagemann G, Bruehl C, Lutzenburg M, Wite OW. Brain hypometabolism in a rat model of chronic focal epilepsy in rat neocortex. Epilepsia 1998;39:339–346.
174. Penner R, Heher E, Dreyer F. Intracellularly injected tetanus toxin inhibits exocytosis in bovine adrenal chromafin cells. Nature Med 1986;324:76–78.
175. Calabresi P, Benedeti M, Mercuri NB, Bernardi G. Selective depression of synaptic transmission by tetanus toxin. A comparative study on hippocampal and neostriatal slices. Neurosci 1989;30:663–670.
176. Bergey GK, Bigalke H, Nelson PG. Differential effects of tetanus toxin on inhibitory and excitatory synaptic transmission in mammalian spinal cord neurons in culture; a presynaptic locus of action for tetanus toxin. J Neurophysiol 1987;57:121–131.
177. Empson RM, Jeffreys JGR. Synaptic inhibition in primary and secondary chronic epileptic foci induced by intrahippocampal tetanus toxin in the rat. J Physiol 1993;465:595–614.
178. Habermann E, Erdmann G. Pharmacokinetic and histoautoradiographic evidence for the intraaxonal movement of toxin in the pathogenesis of tetanus. Toxicon 1974;16:611–623.
179. Schwab ME, Suda K, Thoenen H. Selective retrograde synaptic transfer of a protein, tetanus toxin, subsequent to its retrotransport. J Cell Biol 1979;82:798–810.
180. Liang F, Jones EG. Differential and time-dependent changes in gene expression or type II calcium/calmodulin-dependent protein kinase, 67 kDa glutamic acid decarboxylase, and glutamate receptor subunits in tetanus toxin-induced focal epilepsy. J Neuroscience 1997; 17:2168–2180.
181. Bergey GK, Macdonald RL, Habig WH, Hardegree MC, Nelson PG. Tetanus toxin convulsant action in spinal cord neurons in culture. J Neurosci 1983;3:2310–2323.
182. Jeffreys JGR, Evans BJ, Hughes SA, Williams SF. Neuropathology of the chronic epileptic syndrome induced by intrahippocampal tetanus toxin in the rat: preservation of pyramidal cells and incidence of dark cells. Neuropath Appl Neurobiol 1992;18:53–70.
183. MacVicar BA, Hochman D, LeBlanc FE, Watson TW. Stimulation evoked changes in intrinsic optical signals the human brain. Soc Neurosci Abstr 1990;16:309.
184. Cannestra AF, Black KL, Martin NA, et al. Topographical and temporal specificity of human intraoperative optical intrinsic signals. NeuroReport 1998;9:2557–2563.
185. Cannestra AF, Blood AJ, Black KL, Toga AW. The evolution of optical signals in human and rodent cortex. NeuroImage 1996;3: 202–208.
186. Cannestra AF, Bookheimer SY, O'Farrell A, et al. Temporal and topographical characterization of language cortices utilizing intraoperative optical intrinsic signals. NeuroImage 2000;12:41–54.
187. Cannestra AF, Pouratian N, Bookheimer SY, Martin NA, Becker DP, Toga AW. Temporal spatial differences observed by functional MRI and human intraoperative optical imaging. Cerebral Cortex 2001;11:773–782.
188. Pouratian N, Bookheimer SY, O'Farrell AM, et al. Optical imaging of bilingual cortical representations. Case report. J Neurosurg 2000; 93:676–681.
189. Pouratian N, Sheth SA, Martin NA, Toga AW. Shedding light on brain mapping: advances in human optical imaging. Trends Neurosci 2003;26:277–282.
190. Sato K, Nariai T, Sasaki S, et al. Intraoperative intrinsic signal imaging of neuronal activity from subdivisions of the human primary somatosensory cortex. Cerebral Cortex 2002;12:269–280.
191. Toga AW, Cannestra AF, Black KW. The temporal/spatial evolution of optical signals in human cortex. Cerebral Cortex 1995;5:561–565.
192. Mayhew JEW, Askew S, Zheng Y, et al. Cerebral vasomotion: a 0.1-Hz oscillation in reflected light imaging of neural activity. NeuroImage 1996;4:183–193.
193. Mitra PP, Pesaran B. Analysis of dynamic brain imaging data. Biophys J 1999;76:691–708.
194. Kraemer DL, Spencer DD. Anesthesia in epilepsy surgery, In: Engel JJ, ed. Surgical Treatment of the Epilepsies. New York: Raven Press, Ltd.; 1993:527–538.
195. Schwartz TH, Chen L-M, Friedman RM, Spencer DD, Roe AW. Intraoperative optical imaging of human face cortical topography: a case study. Neuroreport 2004;15:1527–1531.
196. Nelson RJ, Sur M, Felleman DJ, Kaas JH. Representation of the body surface in postcentral parietal cortex of Macaca fascicularis. J Comp Neurol 1980;192:611–643.
197. Felleman DJ, Nelson RJ, Sur M, Kaas JH. Representations of the body surface in areas 3b and 1 of postcentral parietal cortex of cebus monkeys. Brain Res 1983;268:15–26.
198. Jain N, Qi H-X, Catania KC, Kaas JH. Anatomic correlates of the face and oral cavity representations in the somatosensory cortical area 3b of monkeys. J Comp Neurol 2001;429:455–468.
199. Penfield W, Jasper H. Epilepsy and the functional anatomy of the human brain. Boston, Little Brown, 1954.
200. Van Buren JM. Sensory responses from stimulation of the inferior Rolandic and Sylvian regions in man. J Neurosurg 1983;59:119–130.
201. Uematsu S, Lesser R, Fisher RS, et al. Motor and sensory cortex in human: topography studied with chronic subdural stimulation. Neurosurgery 1992;31:59–72.
202. Sur M, Merzenich MM, Kaas JH. Magnification, receptive-field area, and "hypercolumn" size in areas 3b and 1 of somatosensory cortex in owl monkeys. J Neurophysiol 1980;44:295–311.